CHALMERS

Remote Plant Stress Detection in Greenhouse Environments

Master Thesis in Systems, Control and Mechatronics

Lukas Wikander

Department of Signals and Systems
Systems, Control and Mechatronics
Chalmers University of Technology
Gothenburg, Sweden 2016

Remote Plant Stress Detection in Greenhouse Environments

LUKAS WIKANDER

Examiner: Torsten Wik

Supervisor: Daniel Bånkestad

Chalmers University of Technology

Department of Signals and Systems

SE-412 96 Göteborg

Sweden

Telephone + 46 (0)31-772 1000

Department of Signals and Systems
Göteborg, Sweden June 2016

Abstract

To increase greenhouse productivity and reduce power consumption, a large scale lighting control system is sought for. Part of the envisioned lighting control system involves plant stress detection wherefore a novel stress detection method, termed Dynamic Fluorescence Response Analysis (DFRA), is being developed. Enabling DFRA in situations where sunlight is present requires that the method, in its current form, is modified. To this end, several techniques mitigating the unwanted effects of sunlight are developed or investigated in this work. Among these techniques are Fraunhofer Line Discrimination (FLD), an established method for remotely determining photosynthetic activity in plants. It is found that FLD is unsuitable for DFRA without highly precise equipment, as it amplifies noise when used at the time scales required. Furthermore, several signal processing techniques are implemented, extending DFRA to being applicable also in presence of sunlight. The techniques are evaluated and it is found that most of them are overly sensitive to measurement noise, causing the stress diagnosis to be unreliable.

Keywords. Remote sensing, plant stress, dynamic fluorescence response analysis (DFRA), sun-induced chlorophyll fluorescence (SIF), Fraunhofer line discrimination (FLD), signal processing, parametric modelling, system identification

Sammanfattning

För att öka produktiviteten samt minska energiförbrukningen i växthus behövs ett storskaligt reglersystem för växthusbelysningen. Detta reglersystem innefattar stressdetektion hos växter varför en ny stressavkänningsmetod, Dynamisk Fluorescensresponsanalys (DFRA), håller på att utvecklas. För att DFRA skall kunna användas i närvaro av solljus krävs modifikation av metoden. I detta arbete utvecklas eller undersökes därför ett flertal olika sätt att mildra de oönskade effekterna av solljus på DFRA-metoden. Bland dessa finns till exempel Fraunhoferlinjeurskiljning (FLD, för Fraunhofer Line Discrimination), en etablerad metod för att detektera fotosyntetisk aktivitet hos växter på långa avstånd. Slutsatsen är att FLD, utan precis utrustning, inte lämpar sig väl för användning tillsammans med DFRA, då metoden vid de intressanta tisskalorna förstärker brus. Vidare undersöks ett flertal signalbehandlingsbaserade metoder, av vilka de flesta visar sig överkänsliga emot brus, och gör således stressdiagnosen otillförlitlig.

Nyckelord. Fjärravkänning, växtstress, dynamisk fluorescensresponsanalys (DFRA), Fraunhoferlinjeurskiljning (FLD), signalbehandling, parametrisk modellering, systemidentifiering

Acknowledgements

I would like to thank Daniel Bånkestad and Johan Lindqvist for valuable insights, support and guidance during the course of this work, and for always being ready to discuss the topic. I would also like to thank Torsten Wik and Anna-Maria Carstensen for taking interest and for assisting my reasoning at difficult points of the work. Further, I would like to thank Ida Fällström and Grażyna Bochenek for keeping me moving, and, finally, Mei Ha, for proofreading this text.

Lukas Wikander, Gothenburg 30/5/16

Contents

List of Figures

List of Tables

Nomenclature

λ	Wavelength
ρ	Reflectance
θ	Parameter vector
φ	Regressor vector
d	Sunlight
e	Error
g	Plant canopy dynamic system
l	Lamp light
u	Sum of lamp light and sunlight
y	Fluorescence and reflected sunlight
ARX	AutoRegressive with eXogenous input
ChlF	Chlorophyll Fluorescence
FLD	Fraunhofer Line Discrimination
FWHM	Full Width at Half Maximum
LED	Light Emitting Diode
NPQ	Non-Photochemical Quenching
OE	Output Error

PAR Photosynthetically Active Radiation

PQ Photochemical Quenching

PSI PhotoSystem I

PSII PhotoSystem II

SNR Signal-to-Noise Ratio

A mathematical symbol with a hat, e.g. $\hat{\rho}$, indicates that the variable is an estimate of the true variable.

1

Introduction

With automation progressively spreading through a range of industries, the greenhouse industry is quick to follow. In order to match market demands precisely and in a just-in-time way, increased control of crop growth is needed. Further, augmented control of plant growth is expected to reduce power consumption and increase plant growth overall. Chalmers University of Technology and Heliospectra AB are, to this end, jointly developing a biological feedback method to control (or maximise) plant growth, as shown in Figure 1.1. A subcomponent of this biological feedback method is detection of plant stress, whereon the focus of this study lies. As plant stress limits growth, the two are interlaced in such a way that focusing on eliminating stress is a practical goal in itself. Furthermore, it is expected that plant stress detection could be applied to detect abiotic as well as biotic stressors, such as excess light and infections, respectively.

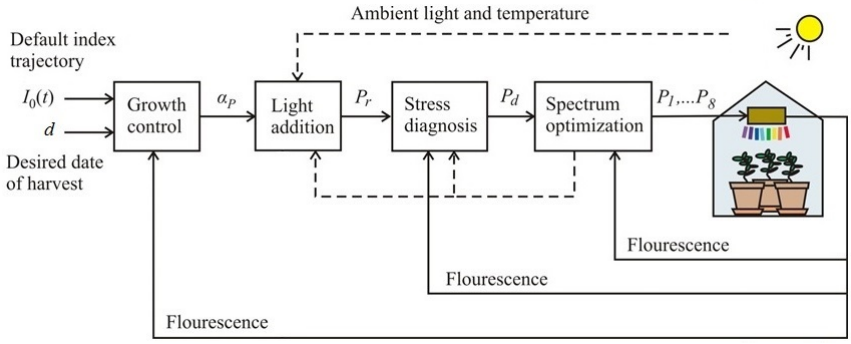

Figure 1.1: Conceptual intelligent light biological feedback system represented as a block diagram. *Source: Torsten Wik*

The method, termed Dynamic Fluorescence Response Analysis (DFRA), is based on analysis of the chlorophyll fluorescence response from plants when subjected to excitation light. Most advantageously, DFRA enables remote stress detection when most traditional fluorescence based stress detection methods require on-leaf measurements. However, the DFRA method, in its current use, requires specialised equipment to function. LED greenhouse lamps are suitable actuators for generating the excitation light as they provide precise control and short response times. Furthermore, LED lamps, as opposed to traditional high-pressure sodium (HPS) lamps, can emit light spectrally distributed in a manner more suited to the method, not to mention the plants themselves. Additionally, spectrometers are needed to collect the various signals needed by the DFRA method.

1.1 Background

In short, the DFRA method comprises fitting of a ready-made dynamical model to collected measurements and subsequent analysis of the properties of the model. As yet, DFRA has only been proven to work in closed lab environments (see [5, 6, 13]). It is not feasible to create such isolated lab conditions in a greenhouse. However, for the method to be applicable for commercial greenhouse operation it must necessarily function also when sunlight is present. Consequently, the focus of this study lies on investigating several techniques mitigating the disturbing influence of sunlight. The following three research questions are posed:

- Does sunlight adversely affect the DFRA model estimation?
- If so, how can these effects be mitigated?
- Which of the investigated countermeasures seems most promising for future use?

1.2 Purpose and aim

The intention of this study is to investigate or develop a number of methods with which sunlight can be accounted for in the DFRA method. The study should investigate at least one method based on spectrometry and, further, at least one based on signal processing.

1.3 Scope

The focus of this study lies on method development, studying how varying sunlight can be accounted for in the DFRA method. Due to this, and to the author's lack of background in biology, reference measurements for assessing plant stress level are not performed.

Instead, results are considered adequate if they are similar to previous experiments made in controlled lab environments. Alternatively, the results should be similar in experiments where the plant stress level can be assumed to be the same.

1.4 Document structure

In Chapter 2, relevant concepts and related research are presented, giving a background to this work. Thereafter follows Chapter 3 which lays forth the methods developed, or investigated, in this work. Following that, the results of using the methods on both simulated and measured data are shown in Chapter 4. The results and methods are discussed in Chapter 5, along with suggestions for future work. Finally, the methods are evaluated and the research questions answered in short as part of Chapter 6.

2

Theory and Related Work

UNDERSTANDING of several biological and signal processing concepts is a necessary prerequisite for being able to follow the majority of this text. Therefore, the most vital ones are presented here. Following this, recent research in related areas, e.g. DFRA and sun-induced fluorescence retrieval, is summarised, giving an overview of the background of this work.

2.1 Theory

This section describes several concepts. Firstly, perhaps the most central one, chlorophyll fluorescence, is described along with a few other biology-related concepts. Secondly, parametric modelling is described in short, with two model structures being described in more detail. Lastly, filtering methods are presented. Some of the concepts shown could appear trivial but are nonetheless included as the fields of biology and signal processing are indeed quite separate.

2.1.1 Chlorophyll fluorescence

Photosynthesis is the chemical process taking place in plants which uses absorbed light energy to convert carbon dioxide and water into storable chemical energy (sugar) and oxygen. Light energy is absorbed in photosystem II (PSII) and photosystem I (PSI) by proteins containing chlorophyll, to drive photochemistry. However, the absorbed light can also be dissipated as heat, a process called *non-photochemical quenching* (NPQ), or be re-emitted as light in the form of *chlorophyll fluorescence* (ChlF). ChlF is emitted at wavelengths between 650-800 nm [3], as can be seen in Figure 2.1.

ChlF has been used for decades to non-invasively measure photosynthetic activity in plants. By exciting ChlF manually with a flash of light, and comparing the ratio between different parts of the response, information regarding the prevalence of NPQ and photochemistry can be gathered. Measurements of this type are normally conducted on-leaf with an instrument creating the exciting flash of light as well as measuring the induced ChlF.

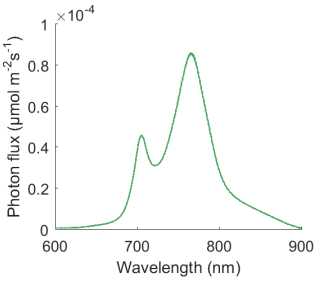

Figure 2.1: Example of chlorophyll fluorescence radiation.

Typically, a sudden increase in light gives rise to a quick response in ChlF intensity which then starts to fall over the course of a few minutes due to an increase in electron transport rates away from PSII (a process known as *photochemical quenching*, PQ), as well as a gradual increase in NPQ. Steady state of the ChlF signal is normally reached after 15 - 20 minutes, however this differs greatly between plant species [16].

2.1.2 Photosynthetically active radiation

In studies on photosynthesis, it is common to measure light to which plants are subjected only in the interval from 400 nm to 700 nm wavelength. Light in this wavelength band is absorbed by cholorophyll pigments in PSII and PSI, and used to drive photosynthesis. This radiation wavelength interval is commonly referred to as Photosynthetically Active Radiation, or PAR [17]. In order for photosynthesis to be active, actinic light - light with sufficient spectral quality and intensity to drive the photochemical reactions - must be present. The limit for light actinism varies with plant species.

2.1.3 Data sampling

In order to handle continuous signals in computers, it is common to convert them into sequences of discrete data points through sampling. Given a continuous signal $x(t)$, values can be collected at N discrete time instants $\{t_1, \ldots, t_N\}$ to form a sampled sequence $\{x(t_1), \ldots, x(t_N)\}$. Often, the same interval between samples is used, such that a sampling interval $\mathrm{T_s}$ can be defined. With such an assumption, notation can be somewhat simplified with the following shorthand:

$$y(n) \triangleq y(t_0 + n\mathrm{T_s}), \quad n = 1, \ldots, N, \tag{2.1}$$

with t_0 denoting the time of the first sample.

2.1.4 System identification

In many engineering problems it is of interest to make predictions, or characterisations of a physical system. If the system being studied is very complex, it can be a time-

consuming or even infeasible task to create a model based on physical insights. In such cases, a predefined model structure can be used, which does not necessarily have a structure matching the system, but which is able to make predictions of the system's behaviour (or output). Given input and output measurement data, $\mathbf{u} \in \mathbb{R}^N$ and $\mathbf{y} \in \mathbb{R}^N$, respectively, a model can be estimated which generates the outputs $\hat{\mathbf{y}} \in \mathbb{R}^N$ such that, e.g.

$$V_N = \sum_{n=1}^{N} (y(n) - \hat{y}(n))^2 \tag{2.2}$$

is minimised.

2.1.5 Parametric model

Given experimental data with consecutive inputs $\mathbf{u}$ and outputs $\mathbf{y}$, a model can be estimated that generates the outputs $\hat{\mathbf{y}}$ from the input sequence $\mathbf{u}$. In the parametric case, the model is estimated given a set of parameters $\theta = [\theta_1 \cdots \theta_M]$, with *a priori* defined M and model structure. The fit percentage for an estimated model is calculated as the normalised root mean square error [27]:

$$\text{fit}[\%] = 100 \left(1 - \frac{\|y - \hat{y}\|}{\|y - \text{mean}(y)\|} \right) \tag{2.3}$$

2.1.5.1 Autoregressive exogenous input model

One such structure, termed ARX for AutoRegressive with eXogenous input, is simple with respect to estimation of model parameters and has the following appearance [12, 14]:

$$y(n) = \frac{B(q)}{F(q)} u(n) q^{-k} + \frac{1}{F(q)} e(n), \tag{2.4}$$

with q being the time shift operator, $e(t)$ the disturbance, B and F polynomials of the transfer function to be estimated, and $k \in \mathbb{Z}^*$ the input delay. This model structure is also known as the equation error model [28].

If the structure is expressed in the form of a difference equation, it becomes clear that estimation of the parameters in an ARX model is simple due to the equation being linear in the parameters:

$$\begin{aligned} y(n) &= b_1 u(n-k) + b_2 u(n-1-k) + ... + b_{n_b} u(n-n_b-k) \\ &\quad - a_1 y(n-1) - ... - a_{n_a} y(n-n_a) + e(n) \\ &= \theta^T \varphi(n) + e(n), \end{aligned} \tag{2.5}$$

where

$$\theta = [b_1 \quad \cdots \quad b_{n_b} \quad a_1 \quad \cdots \quad a_{n_a}]^T \tag{2.6}$$

$$\varphi(n) = [u(n-k) \quad u(n-1-k) \quad \cdots \quad u(n-n_b-k) \quad -y(n-1) \quad \cdots \quad -y(n-n_a)]^T \tag{2.7}$$

Given a data set $\{\mathbf{u},\ \mathbf{y}\}$, a parameter vector estimate $\hat{\theta}$ can, for this structure, easily be identified using the least squares method [12], for example.

2.1.5.2 Output error model

Another model structure is the so called Output Error (OE) model. Its structure is similar to the ARX structure, with the difference that the error $e(t)$ is not fed back into the system. It is covered here as it is the model structure found to give the best fit to the ChlF response in plants studied by previous work [5, 6, 13]. The model has the following structure [12, 14]:

$$y(n) = \frac{B(q)}{F(q)}u(n)q^{-k} + e(n). \tag{2.8}$$

Here, it is not as simple to identify the parameters of the polynomials B and F, as the corresponding difference equation is a nonlinear function of θ. In general, the least squares solution for this case is biased [12] and so an iterative approach must be applied, e.g. gradient descent [14] or the instrumental variables method [12].

2.1.6 Frequency domain representation

A discrete time transfer function $G(q)$ can be represented in the frequency domain by transforming it to $G(z)$ with the Z-transform. Properties of the frequency function $G(z)$ can be studied, such as the input-output magnification of the function, or its input-output phase shift. Studying these frequency-dependent properties can then reveal attributes which would otherwise be difficult to show. As a very basic example, a two sample moving average filter,

$$y(n) = \frac{u(n) + u(n-1)}{2}, \tag{2.9}$$

can be represented by the transfer function

$$G(z) = 0.5 + 0.5z^{-1}. \tag{2.10}$$

The transfer function can then in turn can be shown in a Bode plot, by evaluating the transfer function at $z = e^{j\omega T_s}$, as can be seen in Figure 2.2 (a Bode plot shows the input-output magnification and phase shift of a transfer function as functions of frequency ω). Clearly, the filter admits lower frequency input signals while rejecting higher frequencies — it has a low-pass character.

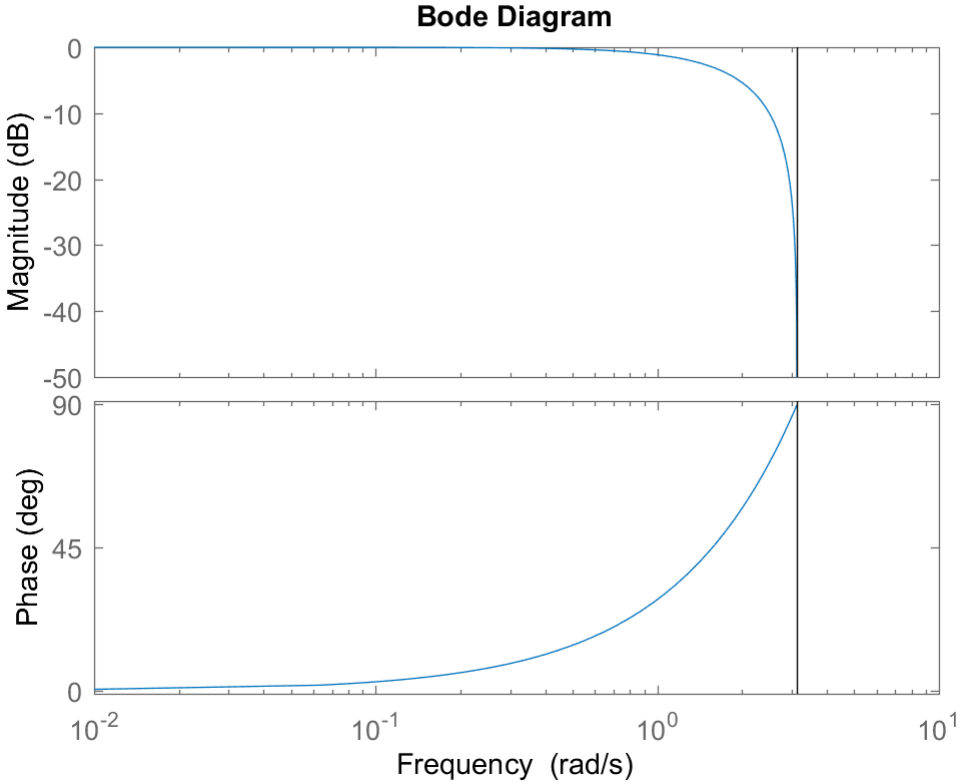

Figure 2.2: Bode plot of a simple two sample moving average filter. The top graph shows the frequency dependent input-output amplification of the filter, while the bottom graph shows its phase shift. The filter admits lower frequencies while attenuating higher frequencies, as is expected of an averaging filter.

2.1.7 Butterworth filter

Filter design is often a compromise between several filter properties. The Butterworth filter design method produces a filter which is maximally flat in the passband (perturbing the frequency content of interest as little as possible) while having a slow roll-off in the stopband [4, 21]. In other words, if the unwanted signal content has frequencies in the same region as the desired signal, it is not attenuated much by the filter.

Using the Butterworth design technique to design a low-pass filter with unity gain in the passband produces a filter with gain according to Equation (2.11). Here, n is the filter order and ω_c the cut-off frequency [21].

$$|G(\omega)| = \frac{1}{\sqrt{1 + \left(\frac{\omega}{\omega_c}\right)^{2n}}} \tag{2.11}$$

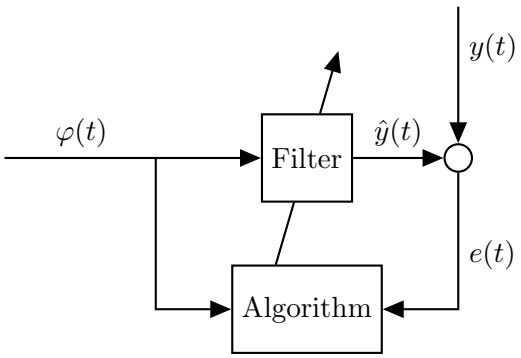

Figure 2.3: General adaptive filter configuration. It is the objective of the adaptive filter to ensure that $\hat{y}(t)$ matches $y(t)$ as closely as possible using $\varphi(t)$ as input, e.g. by minimising the mean square of $e(t)$.

The filter has a gain of 0.5 at the cut-off frequency independently of the filter order, but has an increasing roll-off with increasing order [21].

2.1.8 Adaptive filtering

An adaptive filter is, as the name implies, a filter which changes with time. It operates in a closed loop configuration in some way, and its parameters are changed to achieve a goal (e.g. minimisation of the mean squared error of some signal) via an algorithm, as shown by Figure 2.3. In the case of Figure 2.3, it can e.g. be the task of the adaptive filter to use the input $\varphi(t)$ to minimise the mean square of the error $e(t)$, by ensuring that $\hat{y}(t)$ matches $y(t)$ as closely as possible, for instance by minimising the cost function ξ [21]:

$$\xi = \sum_{k=0}^{n} (y(k) - \hat{y}(k))^2 \tag{2.12}$$

The structure of the filter must be specified *a priori*, i.e. the number of filter parameters N, and, in the parametric modelling case, which parameter vector θ and regressor vector φ to use.

There are two main algorithms for adapting the filter parameters; stochastic gradient and recursive least squares (RLS). The two algorithms have advantages over each other in the form of higher convergence speed (RLS) as opposed to reduced computational complexity (stochastic gradient). To follow the time-varying parameters of a plant canopy as closely as possible the RLS algorithm is chosen for evaluation here. Furthermore, a forgetting factor α can be added to the algorithm, which ensures that previous states of the plant are not overly emphasised. The forgetting factor is essentially a weight which is reduced as samples become older. With forgetting factor, the cost function to be minimised by

the algorithm is instead [21]

$$\xi = \sum_{k=0}^{n} \alpha^{k-n}(y(k) - \hat{y}(k))^2 \tag{2.13}$$

2.1.8.1 The Recursive Least Squares algorithm

The algorithm minimising ξ in Equation (2.13) is shown below. The RLS algorithm is initialised by setting the covariance matrix R_φ and parameter vector $\hat{\theta}$ to

$$R_\varphi(0) = \frac{1}{\delta} I_N \tag{2.14}$$

$$\hat{\theta}(0) = \mathbf{0} \tag{2.15}$$

where δ is a small positive number to indicate a large initial uncertainty. Following the initialisation the following is calculations are repeated for each sample, $n = 1, 2, ...$ [21]:

$$\hat{y}(n) = \hat{\theta}(n-1)\varphi(n) \tag{2.16}$$

$$e(n) = y(n) - \hat{y}(n) \tag{2.17}$$

$$R_\varphi^{-1}(n) = \frac{1}{\alpha}\left[R_\varphi^{-1}(n-1) - \frac{R_\varphi^{-1}(n-1)\varphi(n)\varphi^T(n)R_\varphi^{-1}(n-1)}{\alpha + \varphi^T(n)R_\varphi^{-1}(n-1)\varphi(n)}\right] \tag{2.18}$$

$$\hat{\theta}(n) = \hat{\theta}(n-1) + R_\varphi^{-1}(n)\varphi(n)e(n) \tag{2.19}$$

2.2 Related work

Recent research in related areas is presented below, focusing firstly on methods of retrieval of ChlF from spectral measurements influenced by the severe disturbance of sunlight and secondly on DFRA, a newly developed method for remote detection of plant stress.

2.2.1 Remote sensing of sun-induced fluorescence

Previous work by Maier *et al.* [15] proposes a method for extracting ChlF from air- or spaceborne spectral measurements. Maier *et al.* [15] apply the Fraunhofer line discrimination (FLD) principle to separate ChlF from reflected light. Based on this principle, Rascher *et al.* [24] measure spectral data both at ground level and at a flight height of 3.5 km with the goal of relating ground based field studies and global scale measurements of ChlF to each other.

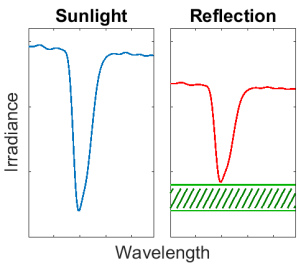

Figure 2.4: Conceptual illustration of FLD. ChlF (green) is added to the reflected sunlight (red).

FLD utilises the absorption band of atmospheric oxygen at 762 nm, where the ratio between fluorescence and reflected sunlight is relatively high, to extract the chlorophyll fluorescence signal. By studying the ratio between the incident irradiance in the absorption band and that just outside it, and comparing it to the corresponding ratio for the emitted and reflected radiance from the plant canopy, the ChlF signal can be extracted. In essence, a system of equations can be posed as

$$L_i = R \cdot E_i + F \tag{2.20}$$

$$L_o = R \cdot E_o + F \tag{2.21}$$

and then solved for F. L denotes radiance (to the right in Figure 2.4) and E denotes incident sunlight (to the left in Figure 2.4). R denotes reflectance. The subscripts $\{i,o\}$ denote that a value is taken inside or outside the absorption band, respectively.

Rascher *et al.* [24] improve upon the method laid forth by Maier *et al.* [15], by accounting for variation of ChlF intensity around the O_2-A (oxygen has several absorption bands, however only the A and B bands are in the range of ChlF) absorption band at 760 nm. Furthermore, Rascher *et al.* [24] use atmospheric modelling software (MODTRAN-5) — based on work by Berk *et al.* [2] — to accurately account for atmospheric extinction and reflection of light, which is necessary for remote measurements. Rascher *et al.* [24] use interpolation over a second order curve to estimate the reflectance in the absorption band, thus correcting for varying fluorescence and reflectance over the band. The low model order is motivated further by other, more specialised, research in the area [9, 18] where higher model orders are shown to be necessary only for the O_2-B absorption band (at 687 nm), and being more sensitive to sensor noise otherwise.

The method shown in the work by Rascher *et al.* [24] is, among others, evaluated in a study by Meroni *et al.* [19]. A comparison is made between several methods based on the original FLD method developed by Plascyk and Gabriel [22]. It is found that the best choice of method depends very much on available instrumentation, with some methods only being applicable with highly precise instruments. Based on the evaluation made by Meroni *et al.* [19], the particular method implementation shown by Rascher *et al.* [24] ("3FLD" in [19]) is chosen for use in this work due to the more advanced methods requiring high precision instruments. The details of this method are found in Section 3.3.2.1.

A study by Julitta *et al.* [10] evaluates the performance of four spectrometers in extracting sun-induced fluorescence with the FLD principle. It is found that a very high spectral resolution is needed (≤ 1 nm full width at half maximum, FWHM) to accurately capture the fluorescence signal. The following equation for calculating absorption band depth is used to evaluate performance of a spectrometer in detecting the absorption band [10]:

$$\text{Depth}[\%] = 100 \cdot \frac{L_{out} - L_{in}}{L_{out}}, \tag{2.22}$$

with $L(\lambda)$ being the incident irradiance. The two points at which values are taken are defined as

$$L_{out} = \max_{\lambda \in (750,755)} L(\lambda), \quad L_{in} = \min_{\lambda \approx 760} L(\lambda). \tag{2.23}$$

A value of 75 % is said to represent an adequate spectrometer according to Julitta *et al.* [10]. Using a spectrometer with spectral resolution of 0.2 nm, the depth of the O_2-A absorption band was estimated to 81 % by Julitta *et al.* [10]. The same value for a spectrometer with resolution 1 nm was 77 % and 49 % for a spectrometer with 5.5 nm resolution. In other words, using spectrometers with too low spectral resolution results in sunlight still being present in the calculated fluorescence value. Julitta *et al.* [10] finds that, for the O_2-B absorption band, the accuracy of the extracted ChlF value depends heavily on spectral resolution. The spectral resolution limit of 1 nm is more harsh in this case, with the accuracy deteriorating quickly with decreasing resolution. It should be mentioned that Julitta *et al.* [10] use a threshold of $3\,\mathrm{mW\,m^{-2}\,sr^{-1}\,nm^{-1}}$, based on a study by Rossini *et al.* [25], to determine the corresponding 75 % threshold.

Focus of the research on retrieval of sun-induced fluorescence appears to lie on the steady-state absolute level of ChlF to determine photosynthetic activity rather than rapid changes in ChlF. Consequently, [9, 10, 15, 18, 24, 25] do not have an upper limit on e.g. integration or sampling times. This enables noise removal through e.g. sample averaging, as performed by Julitta *et al.* [10], without loss of information.

2.2.2 Dynamic chlorophyll *a* fluorescence response analysis

Carstensen *et al.* [6, 7], and related work by Lindqvist [13], describe a novel method for remote detection of plant stress termed Dynamic Fluorescence Response Analysis. The method involves fluorescence induction from a distance of 1-2 m with an LED lamp, and subsequent analysis of the measured slow fluorescence dynamics. By fitting an OE model (see Section 2.1.5) to the ChlF response to a step excitation, frequency dependent properties of the modelled system can be studied. The step excitation is relatively small compared to the constant background light used. Carstensen *et al.* [5] shows that a lower model order is sufficient to model a plant under conditions with too much light. Lindqvist [13] further shows that water induced stress affects the model order and phase shift of the identified system. An OE model with three poles and three zeros is sufficient to model the fluorescence response of the plant canopy when the plants are not stressed. When the plants are overly stressed, only two poles and two zeros are needed and during extreme stress, a single pole is enough. The analysis is performed through visual inspection of the model phase shift plot, with the gain being mostly ignored due to its dependency on sensor placement and spatial configuration of the canopy. The only exception is that the resonance frequency (frequency where the amplitude response is highest) is occasionally used to characterise the level of stress.

PSII is non-linear in its response to changes in light. It has been suggested by Carstensen *et al.* [6] that the ChlF response exhibits the characteristics of a buffer system with feed-

back. Furthermore, the system varies with time, depending on a multitude of factors, e.g. plant stress or light level. Due to the non-linearity and time-variance of the modelled system, it is necessary to use very specific parts of the ChlF response for system identification. As an example, the response to upward steps is different than that to downward steps, wherefore upward and downward steps are not used in the same system identification data sets. Moreover, there exists a deadzone for low incident PAR, as stated in Section 2.1.2, where a certain level of photon flux is necessary for photochemical reactions to take place. To avoid this non-linearity of the modelled system, a background light level exceeding the required level is always used for DFRA. Additionally, the same estimation and validation data sets are used for DFRA model estimation, due to the time-varying nature of the modelled system in conjunction with the time invariance of the estimated model.

It is shown by Lindqvist [13] that the stress dependent change of the phase function varies with plant species. This means that tailoring of the DFRA method to each individual species of plant is required.

3

Methods, Materials and Experiments

ACCOUNTING for reflected sunlight in measurements of chlorophyll fluorescence is a daunting task. As shown in Chapter 2, it is indeed an area where significant scientific advances are still being made. The main cause of difficulty is the fact that the ChlF constitutes merely 1-5 % of the plant canopy radiance [19], making extraction of the fluorescence difficult. Several methods separating the ChlF signal from reflected sunlight are applied in this work, as described in this chapter.

3.1 Material

Firstly, collection of measurement data is presented. In order to measure ChlF, spectrometers are used in this work, mounted on a rig together with optic fibres and LED greenhouse lamps. The lamps are used to excite a ChlF response in a canopy of basil plants which is then measured by one of the spectrometers. Furthermore, the sunlight and excitation light are measured by two other spectrometers.

3.1.1 Spectrometers

All measurement data in this thesis have been collected in a commercial greenhouse with a set-up utilising three spectrometers. The spectrometers are installed to measure incoming (lamp and sun) light, fluorescence contaminated by reflected sunlight, and solely sunlight, respectively. The first of the spectrometers, M1 in Table 3.1, is connected with an optic fibre and cosine corrector in order to collect incoming light from about

Table 3.1: Instrument data for spectrometers used in experiments. All instrument data save for the absorption band depth is supplied by the manufacturer. If two values exist for a parameter, this indicates that the second value was used for the corresponding second experiment.

Reference name Measured spectrum	M1 Irradiance at canopy level	M2 Radiance from canopy	Jaz Irradiance above lamp
Spectrometer model (Ocean Optics)	Maya2000 Pro	Maya2000 Pro	Jaz
Wavelength resolution (FWHM) [nm]	1.85	1.85	1.06
Wavelength range [nm]	199.1-1116.7	198.2-1085.6	339.7-1022.4
Absorption band depth [%]	79	-	63
Fibre diameter [µm]	600 / 50	600	3900
Cosine corrector	Yes	No	Yes
Field of view	180°	20°	180°

12 cm above the plant canopy. The second spectrometer (M2 in Table 3.1) is used, also with an optic fibre, to measure reflected light and fluorescence. The spectrometer is fitted with a Gershun tube to limit its field of view to a 0.35 m^2 area of the canopy (20° field of view from a height of 81 cm). The third spectrometer, Jaz in Table 3.1, is used to measure only sunlight, with an attached cosine corrector, approximately 10 cm above the lamp(s).

To further remove noise from spectrometer measurements, spectra are collected in total darkness to be subtracted from the data post measurement. The darkness spectra were not collected at the experiment site due to the time consuming nature of their collection.

3.1.2 Excitation light

The lamp(s) used for inducing fluorescence responses, Heliospectra LX602, contains LEDs of three types: blue (450 nm), red (660 nm) and white (5700K) LEDs. Only the blue LEDs are used for excitation, as they are furthest from the ChlF wavelength band and therefore do not interfere with ChlF measurements. Figure 3.1 below shows the spectrum of one lamp when using only the 450 nm LEDs, at maximum intensity.

With the lamp settings used (450 nm LEDs at maximum), one lamp outputs 55.8 µmol m^{-2} s^{-1} PAR of blue light at canopy level when turned on. The input signal used (one lamp) is a square wave with a period of 120 s, as shown in Figure 3.2.

When a background light is used, it is provided by a second, similar, lamp, for which

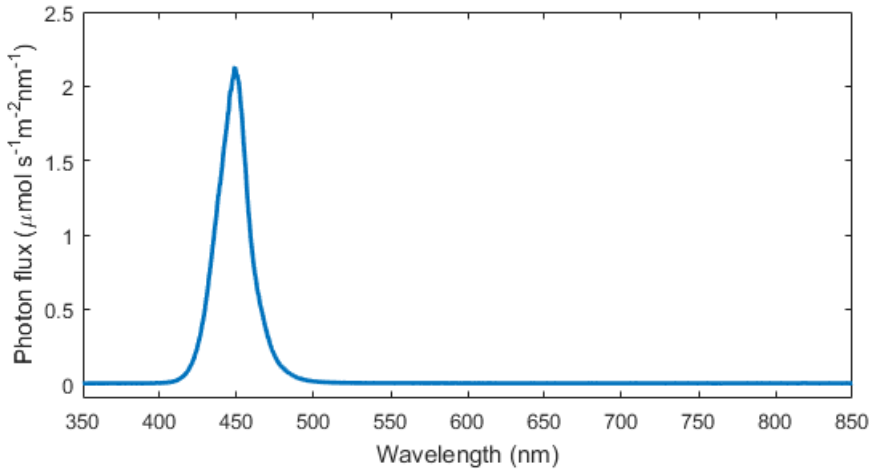

Figure 3.1: Wavelength spectrum of excitation light.

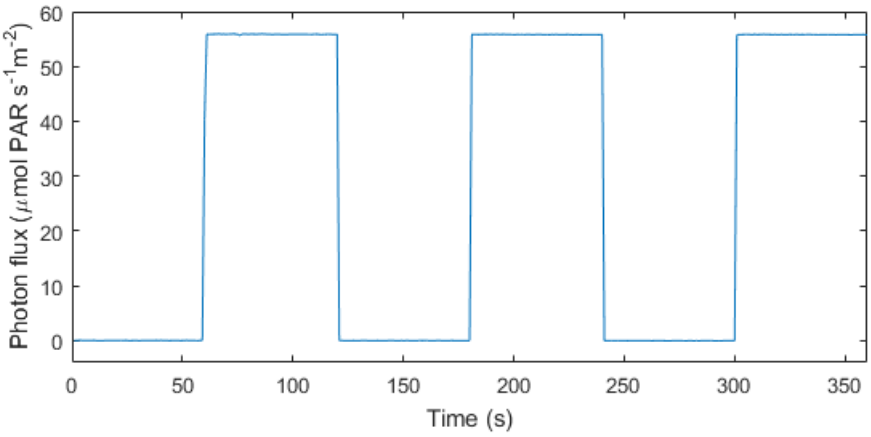

Figure 3.2: Square wave used as input signal to excite ChlF response.

the spectrum can be seen in Figure 3.3. The intensity of the lamp is set according to what is necessary (see Section 3.2).

The LX602 lamps have temperature controllers for which references in the experiment are set at 8 °C, implying that the fans in the lamps are running continuously and thus keeping the LED temperature constant and, further, affecting the voltage over the LEDs equally at all times during an experiment.

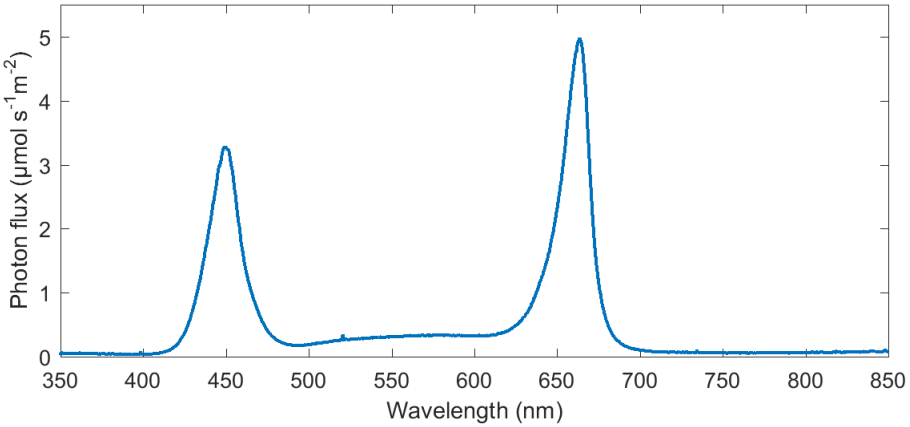

Figure 3.3: Spectrum of light used to create a background level with PAR similar to sunlight, added with the excitation signal from Figure 3.1.

3.1.3 Plant species

All experiments have been conducted on basil (*Ocimum Basilicum*, 'Aroma2') plants, as they were readily available to perform experiments on at the greenhouse. Furthermore, previous work in this research project [5, 13] has focused on this particular cultivar of basil. Experiments are conducted on plants of different age in the first experiment and on only one age-group of basil in the second experiment. The basil plants in the second experiment were approximately three days from harvest.

3.2 Experiments

Two experiments were performed in a commercial greenhouse, owned by Spisa Smaker AB, in Påarp, Sweden (56°01′38″ N, 12°48′54″ E). The first experiment took place between 11:25 and 17:01 the 11$^{\text{th}}$ of February 2016. A second experiment was performed the 20th of April the same year, between 12:20 and 17:28. In February, the weather was mostly overcast, however, intermittently there were a few minutes of sunlight. In April, on the other hand, scarcely a single cloud was visible during the entire day. The approximate sunlight photon flux at canopy level was 70 µmol m^{-2} s^{-1} PAR in February and 500 µmol m^{-2} s^{-1} in April.

The second experiment was conducted to verify results from the first and, further, to collect data with an actinic sunlight level comparable to the background light used by Lindqvist [13].

3.2.1 February experiment

ChlF was induced through repeated series of three light level steps, from the lamp being completely off to having the blue LEDs at full power, as seen in Figure 3.2. Thick insulation curtains were present during the entire experiment, diffusing the incident sunlight. The spectrometer integration times were kept at a constant level during each experiment run. Sampling times were changed several times during the experiment, however within one series of steps the sampling time was kept constant. The two sampling times used were 0.8 s and 1 s, generally longer during the later hours to allow for longer spectrometer integration times.

Some measurements were corrupted by activation of the greenhouse HPS lamps. These measurements were discarded as the HPS lamps radiate light at the ChlF wavelengths.

3.2.2 April experiment

Excitations in this experiment were supplied as three series of 30 consecutive steps, followed by three shorter series used for experiment verification. The first series of step excitations was performed while the greenhouse curtains were in place, in effect providing some optical diffusion lowering the effects of reflections and shading. The second series was performed with the curtains removed, giving a background sunlight level of nearly $900\,\mu\mathrm{mol\,m^{-2}\,s^{-1}}$ PAR. The third was performed with two excitation lamps to attain a larger excitation signal ($89\,\mu\mathrm{mol\,m^{-2}\,s^{-1}}$). Following these series, three shorter experiments with one excitation lamp were performed, first with a black cover admitting a mere $0.3\,\mu\mathrm{mol\,m^{-2}\,s^{-1}}$ PAR of sunlight, then without the cover and finally with the cover again. While using the cover, background light was supplied by the second lamp, mimicking (approximately) the amount of PAR supplied by the sun at that time as a constant background light, between150 and $200\,\mu\mathrm{mol\,m^{-2}\,s^{-1}}$ PAR. The spectrum of the background light can be seen in Figure 3.3.

During all the step series, the integration times were changed in an automated fashion to optimise signal strength and avoid spectrometer saturation.

3.3 Methods

Four methods are applied and evaluated in this work. The first two are related to the area of spectrometry, while the second two are based upon signal processing concepts. The first two methods are:

- Fraunhofer line discrimination (FLD), Section 3.3.2.1
- Spectral quotient, Section 3.3.2.2

These two methods operate only on a single sample, but more extensively within one spectrum. In contrast, the second two methods operate over several samples. They are:

- Curve fitting disturbance removal, Section 3.3.3.1
- Parametric model extension, Section 3.3.3.2

The first two methods are used together with OE model estimations for DFRA stress diagnosis. The latter two are evaluated with both OE and ARX models, as it is reasoned that their application might create some error which does not conform to the OE structure. Furthermore, the latter two are evaluated with simulation data to attest their validity. Additionally, these two methods are based upon a measurement model, which is presented in Section 3.3.1 below instead of in conjunction with the corresponding sections, in order to give the reader better understanding.

3.3.1 Measurement model

Sunlight is a disturbance in two manners. Firstly, as sunlight has spectral content in the same waveband as the ChlF signal, it all but overwhelms the signal of interest. Secondly, the sunlight induces ChlF and, hence, acts as an input disturbance to the system which is to be modelled, potentially interfering with identification of the system.

The wavelength dependent, time-varying dynamic ChlF response (y_f) from PSII to input PAR (u) is modelled by the operator g acting on the input u:

$$y_f(\lambda,n) = g(u(\lambda,n),\lambda,n), \tag{3.1}$$

with λ being wavelength and n being sample number. u comprises the sum of lamp light $l(\lambda,n)$ and sunlight $d(\lambda,n)$ such that

$$u(\lambda,n) = l(\lambda,n) + d(\lambda,n). \tag{3.2}$$

In the ChlF wavelength band, $\lambda \in (650,800)$, the spectrometer *measurements* $y(\lambda,n)$ contain both ChlF and reflected sunlight. Within this wavelength band, the lamp has been assumed not to interfere wherefore only the reflection of sunlight is accounted for. The measured radiance y is then

$$y(\lambda^*,n) = \begin{cases} g(u(\lambda,n),\lambda^*,n) + R(\lambda^*) \cdot d(\lambda^*,n) & \text{if } \lambda^* \in (650,800) \\ R(\lambda^*) \cdot u(\lambda^*,n) & \text{if } \lambda^* \notin (650,800) \end{cases}, \tag{3.3}$$

where $R(\lambda^*)$ is the wavelength dependent reflectance of the plant canopy. Outside the ChlF interval, the measured values are assumed entirely free of ChlF.

As the signals are quite burdensome to handle when they are dependent on wavelength as well as time, it is convenient to study them over wavelength intervals instead. A signal

$x(n)$ is thus formed from the corresponding $x(\lambda,n)$ based on a chosen interval (λ_1,λ_2) in the following manner:

$$x(n) = \int_{\lambda_1}^{\lambda_2} x(\lambda,n)d\lambda \tag{3.4}$$

where λ_1 and λ_2 are chosen according to what interval is of interest. The block diagram in Figure 3.4 models the measured signals, and is used as basis for the signal processing based methods described in Section 3.3.3. Here $y(n)$ is the measured ChlF on the interval $\lambda \in (735,755)$ as well as the reflected light within that interval.

The quantity $d(n)$ is measured in two different manners. Firstly, it is measured directly by the topmost spectrometer collecting only sunlight. For that spectrometer, the spectra collected are integrated according to Equation (3.4) over the PAR interval. Secondly, in order to minimise the number of spectrometers used, the sunlight signal is calculated from the spectrometer facing the canopy, by integrating over the interval 850 - 1000 nm. Naturally, this signal does not have the correct magnitude, however this is compensated for by an overestimation of the reflectance (see Equation (3.24)).

In the measurement model, ρ is the fraction of sunlight added to the collected measurements. Remember that the lamp light contains no light in the ChlF wavelengths and does therefore not pass through the ρ block in Figure 3.4. In fact, ρ is the product of two factors:

$$\rho = f \cdot R \tag{3.5}$$

where f is the ratio between sunlight in the ChlF wavelengths and sunlight in the interval used to create the sunlight signal, i.e. the portion of the sunlight signal disturbing the ChlF signal. In other words,

$$f(n) = \frac{\int_{735}^{755} d(\lambda,n)d\lambda}{\int_{\lambda_1}^{\lambda_2} d(\lambda,n)d\lambda} \tag{3.6}$$

The wavelength dependency of R is ignored here as the interval is small. It can be seen in Figure 3.4 and Equation (3.3) that $y(n)$ is assumed to be a linear composition of fluorescence and reflected sunlight. Both $d(n)$ and $l(n)$ are integrated over the PAR interval as per Equation (3.4). In some cases it is not possible to calculate f. Furthermore, it is only possible to estimate R. For convenience, R and f are therefore treated as a unit, ρ, to be estimated.

3.3.2 Spectral data treatment methods

Two of the methods used operate on a single sample only, and utilise spectral information within that sample to deduce e.g. ChlF. These methods are presented here, starting with FLD which exploits the atmospheric absorption band caused by oxygen. The second method, termed spectral quotient, is similar in concept but uses intervals instead of specific wavelengths.

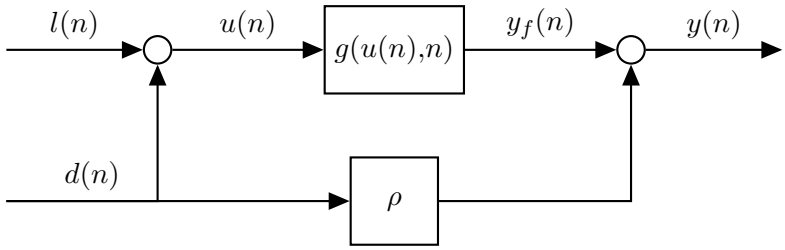

Figure 3.4: Measurement model.

3.3.2.1 Fraunhofer line discrimination

In order to extract the relatively weak fluorescence signal from measurements contaminated by sunlight, it is advantageous to use the O_2-A absorption band as described in Section 2.2.1. The method, known as Fraunhofer line discrimination, relies on the fact that the ratio between the shoulders of the absorption band and the bottom of the band should be the same, both for direct and reflected sunlight. However, the ratios differ in measurements of reflected light from a plant canopy due to the addition of ChlF. Thus, the remainder from comparison between the ratios is determined by the ChlF signal.

The fluorescence intensity, F, inside the absorption band is calculated according to (3.7) [9, 24].

Table 3.2: FLD quantities $V_j(n)$ and corresponding signals.

$V_j(n)$	$x(\lambda,n)$
$E_j(n)$	$u(\lambda,n)$
$L_j(n)$	$y(\lambda,n)$
$L_j^p(n)$	$S(\lambda,n) \cdot d(\lambda,n)$
$\tau_j(n)$	$\tau(\lambda,n)$
$S_j(n)$	$S(\lambda,n)$

$$F_i(n) = B\frac{X_i(n)(E_o(n) + X_o(n)S_o(n)) - AX_o(n)(E_i(n) + X_i(n)S_i(n))}{B(E_o(n) + X_o(n)S_o(n)) - A(E_i(n) + X_i(n)S_i(n))}, \tag{3.7}$$

where the i and o subscripts indicate that a value is taken inside or outside the absorption band, respectively. A full derivation of this equation is found in Appendix A. The values are calculated from Equations (3.8) - (3.10), where V_j ($j \in i,o$) and $x(\lambda,n)$ are replaced with the quantities shown in Table 3.2.

$$V_i(n) = \frac{1}{\lambda_2 - \lambda_1}\int_{\lambda_1}^{\lambda_2} x(\lambda,n)d\lambda \tag{3.8}$$

$$V_o(n) = \frac{1/2}{\lambda_4 - \lambda_3}\int_{\lambda_3}^{\lambda_4} x(\lambda,n)d\lambda + \frac{1/2}{\lambda_6 - \lambda_5}\int_{\lambda_5}^{\lambda_6} x(\lambda,n)d\lambda \tag{3.9}$$

$$X_j(n) = \pi\frac{L_j(n) - L_j^p}{\tau_j} \tag{3.10}$$

where

$$\begin{aligned} \lambda_1 &= 759\,\text{nm}, \quad \lambda_3 = 757\,\text{nm}, \quad \lambda_5 = 768\,\text{nm} \\ \lambda_2 &= 763\,\text{nm}, \quad \lambda_4 = 751\,\text{nm}, \quad \lambda_6 = 773\,\text{nm} \end{aligned} \tag{3.11}$$

L_j^p is the path scattered radiance and τ_j is the transmittance of the atmosphere in the upward direction. $S_j(n)$ is the spherical albedo (fraction of reflected sunlight which is scattered by the surrounding atmosphere into the sensor).

B in Equation (3.7) is the factor relating ChlF intensity inside and outside the absorption band, and A is the factor between the reflectance of the canopy inside and outside the absorption band, i.e.

$$F_i(n) = BF_o(n), \quad R_i = AR_o, \tag{3.12}$$

again with the same intervals.

For this work it is assumed that $\tau_j = 1$, and consequently $S_j = 0$, and further that L_j^p is close to zero as the distances involved are not very large (these assumptions are also supported by Julitta *et al.* [10], Meroni *et al.* [19] for the "centimeters to meters" canopy level range). These assumptions are necessary in order to avoid using expensive atmospheric modelling software. Furthermore, it is assumed that $B = 0.8$ based on [1, 23]. Consequently, Equation 3.7 reduces to the following:

$$F_i = \pi B \frac{L_i E_o - A L_o E_i}{B E_o - A E_i} \tag{3.13}$$

The method described above is entirely based on radiometrical research and removes a very large portion of sunlight reflections. There are, however, some assumptions that can be altered to improve the performance of this method.

Modified assumptions

Equation (3.7) is based on an approximation of the reflectance, which is not readily available, with apparent reflectance. The apparent reflectance, which is the quotient between incident light and radiant light (i.e. it includes fluorescence), is not well suited to the DFRA method, as the method uses relative changes rather than absolute levels.

In order to circumvent the use of apparent reflectance, another set of assumptions can be made. Firstly, the measurement model, which Equation (3.7) is based upon, i.e.

$$L(\lambda) = L^p(\lambda) + \frac{1}{\pi} \frac{\left(E^R(\lambda) + F(\lambda)\right) \tau(\lambda)}{1 - S(\lambda) R(\lambda)}, \tag{3.14}$$

is used. Here, $E^R(\lambda)$ is the pure reflected sunlight, which is not measured, and otherwise the notation is the same as above. Again, it is assumed that the distances involved are short and that consequently

$$L^p(\lambda) = 0, \quad \tau(\lambda) = 1 \implies S(\lambda) = 0, \tag{3.15}$$

Secondly, it is assumed that

$$F(\lambda) = F_0 + k_F(\lambda - \lambda_0), \tag{3.16}$$

where k_F is taken from known ChlF spectra. Finally, it is assumed that the reflectance can be modelled as

$$R(\lambda) = \frac{E^R(\lambda)}{E(\lambda)} = R_0 + k_R(\lambda - \lambda_0) \tag{3.17}$$

Equations (3.14)-(3.17) together pose a system of equations with unknowns F_0, R_0 and k_R, which can be calculated by using measurements from three different wavelengths. So far the method is similar to what Meroni *et al.* [19] name the cFLD method, which is described in [8, 20]. However, to further minimise the effects of measurement noise, measurements are instead taken over the interval 756 nm - 761 nm and the three unknowns are calculated by least squares. These assumptions improve the performance of FLD, however, the spectrometers used do not have sufficient spectral resolution for it to be possible to remove all of the sunlight in this way. Furthermore, when measuring solar induced fluorescence stable atmospheric conditions are assumed, something which is not always the case. It is possible that some ChlF dynamics could be excited by sunlight, perturbing the DFRA model estimate. Moreover, using two different spectrometers with independent measurement noises in conjunction with FLD creates a great deal of noise in the output data, as will be seen in Chapter 4.

3.3.2.2 Spectral quotient

The signal processing based methods, which will be described in the next section, are sensitive to relative sensor placements. FLD, albeit less sensitive to sensor placement, is highly sensitive to measurement noise. This sensitivity is amplified by the use of several spectrometers for which the measurement noises, naturally, are independent. For these reasons, a method which utilises one spectrometer to extract the ChlF signal was developed. Naturally, the spectrometer of choice is the one facing the canopy as it is the only one receiving ChlF.

Looking at one step, if n_s is the sample at which the step occurs, the measured outputs are

$$y(\lambda,n) = \begin{cases} g(d(\lambda,n),\lambda,n) + R(\lambda) \cdot d(\lambda,n) & \text{if } n < n_s \\ g(u(\lambda,n),\lambda,n) + R(\lambda) \cdot u(\lambda,n) & \text{if } n \geq n_s \end{cases} \tag{3.18}$$

where g is zero outside the ChlF interval. The quantity of interest is $g(l(\lambda,n),\lambda,n)$, when $n \geq n_s$ (for simplification, the integral of $g(l(\lambda,n),\lambda,n)$ over $\lambda \in (735,755)$ is instead sought for - it is equivalent when looking at ChlF dynamics). Assuming that the plants' response to the lamp light can be decoupled from that to the sunlight, which is the case when the sunlight does not induce any dynamic ChlF response, the plants' ChlF response to the lamp can be modelled separately from the plants' response to the sunlight through

$$g(u(\lambda,n),\lambda,n) = g(l(\lambda,n),\lambda,n) + g(d(\lambda,n),\lambda,n). \tag{3.19}$$

This means that, after a step, the signal

$$y(\lambda,n) = g(l(\lambda,n),\lambda,n) + g(d(\lambda,n),\lambda,n) + R(\lambda) \cdot d(\lambda,n), \quad \lambda \in (735,755). \tag{3.20}$$

The sum $g(d(\lambda,n),\lambda,n)+R(\lambda)\cdot d(\lambda,n)$ in Equation (3.20) can be calculated for the interval $\lambda \in (735,755)$ as

$$\int_{735}^{755} \Big(g(d(\lambda,n),\lambda,n) + R(\lambda)\Big)d\lambda = Q \int_{800}^{1000} d(\lambda,n)d\lambda, \tag{3.21}$$

where Q is the spectral quotient defined below. If the sunlight can be assumed to have a constant spectral distribution, Q can be calculated from the measurements taken before the step occurs, as an average over all samples $n < n_s$:

$$Q = \frac{1}{n_s - n_0} \sum_{k=n_0}^{n_s} \frac{\int_{735}^{755} \Big(g(d(\lambda,k),\lambda,k) + R(\lambda) \cdot d(\lambda,n)\Big)d\lambda}{\int_{800}^{1000} R(\lambda) \cdot d(\lambda,k)d\lambda}. \tag{3.22}$$

The integrand in the denominator is in fact equal to the measurement $y(\lambda,n)$ as there is no ChlF in that interval. The integrand in the numerator is recognised from Equation (3.18) and is also known. Equations (3.20) - (3.22) together make it possible to calculate $g((\lambda,n),\lambda,n)$ on the interval $\lambda \in (735,755)$ for samples $n \geq n_s$:

$$\int_{735}^{755} g(l(\lambda,n),\lambda,n)d\lambda = \int_{735}^{755} y(\lambda,n)d\lambda - Q \int_{800}^{1000} y(\lambda,n)d\lambda, \tag{3.23}$$

The assumption imposed upon the spectral quotient Q is violated in situations where the spectral distribution of the measured spectrum changes with time. This is the case when e.g. clouds interfere with the incoming sunlight for a part of the step.

3.3.3 Signal processing methods

The methods in this section operate over several consecutive samples and not to a great extent over wavelength, instead using wavelength intervals to create signals in the time domain (refer to Section 3.3.1). Equation (3.4) shows how the signals are formed, for incoming light the PAR interval is used and for ChlF the interval $\lambda \in (735,755)$ is used. To evaluate the theoretical validity of the methods put forth in this section, and to show and understand in which situations they are applicable, the methods are tested by simulation (see Section 3.3.4) in addition to being used on measurement data. All measurement data are filtered with a fifth order band-pass Butterworth filter, with pass band from $0.01\,\mathrm{rad\,s^{-1}}$ to $1\,\mathrm{rad\,s^{-1}}$ based on the interval of interest suggested by [13].

3.3.3.1 Curve fitting disturbance removal

To remove the reflected sunlight from the measured output, the following method was applied. The disturbance $d(n)$ multiplied by a factor $\hat{\rho}$, estimating the reflectance of the canopy, is subtracted from the measurements as shown in Figure 3.5 below.

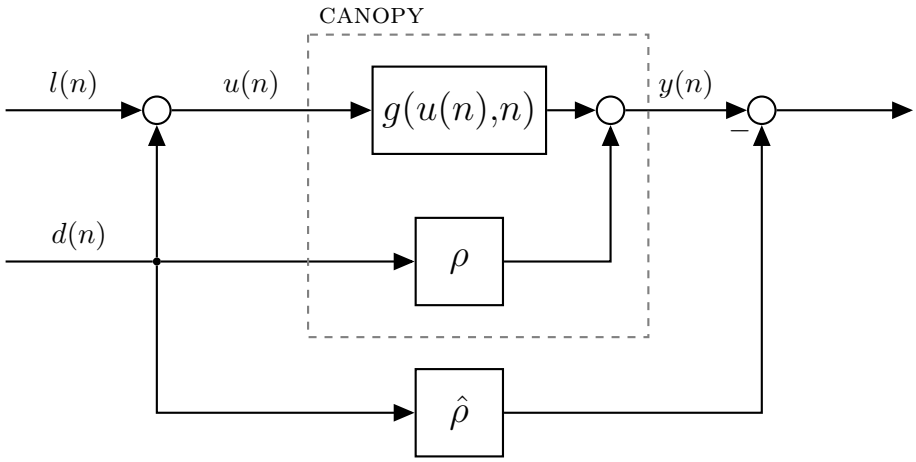

Figure 3.5: Estimation of canopy reflectance.

Ideally, $\hat{\rho}$ should match ρ. However, since ρ is not available, $\hat{\rho}$ can instead be calculated such that the squared difference between $y(n)$ and $\hat{\rho}d(n)$ is minimised:

$$\min_{\hat{\rho}} \left(y(n) - \hat{\rho}d(n)\right)^2 \tag{3.24}$$

Further analysis and details of the method can be found in Appendix C. In short, the estimated $\hat{\rho}$ fulfilling Equation (3.24) depends, to a small degree, on the fluorescence response to $u(n)$, meaning that $\hat{\rho}$ is not truly equal to the reflectance ρ. In other words, some sunlight still remains after this method has been applied.

3.3.3.2 Parametric modelling

Ideally, the estimated reflectance $\hat{\rho}$ should be equal to ρ, since otherwise not all reflected sunlight can be removed. It is therefore desirable to eliminate the mismatch of $\hat{\rho}$. However, this requires knowledge (or an estimate) of the function $g(u(n), n)$, due to the ChlF response to sunlight not being static as is the case with pure reflection. Given disturbance $d(n)$ and output data $y(n)$, a transfer function $\hat{g}$ of the system can be estimated together with a model of the reflection. Using a model order of three poles and three zeros as suggested by Lindqvist [13], with sunlight as disturbance and input signal, the difference equation for $y(n)$ becomes

$$\begin{aligned} y(n) = \theta^T\varphi(n) = (b_0+\rho)d(n) + (\rho a_1 + b_1)d(n-1) + (\rho a_2 + b_2)d(n-2) \\ + (\rho a_3 + b_3)d(n-3) + b_0 l(n) + b_1 l(n-1) + b_2 l(n-2) + b_3 l(n-3) \\ - a_1 y(n-1) - a_2 y(n-2) - a_3 y(n-3) \end{aligned} \tag{3.25}$$

with the parameter vector θ given by

$$\theta = [a_1 \quad a_2 \quad a_3 \quad \rho{+}b_0 \quad \rho a_1{+}b_1 \quad \rho a_2{+}b_2 \quad \rho a_3{+}b_3 \quad b_0 \quad b_1 \quad b_2 \quad b_3]^T \tag{3.26}$$

and with the regressor vector φ defined by

$$\varphi(n) = [-y(n-1) \quad -y(n-2) \quad -y(n-3) \quad d(n) \quad l(n) \quad u(n-1) \quad u(n-2) \quad u(n-3)]^T \tag{3.27}$$

where the parameters $\rho a_i + b_i,\ i \in \{1,2,3\}$ arise from the fact that the signal $y(n)$, which is contaminated by reflection, is not fed back into the system. The signal that is fed back is in fact $y(n) - \rho d(n)$. With noise being more prevalent in this case compared to Lindqvist [13], a model of lower order is also used in some cases. Reducing the number of poles and zeros to two, lowers the likelihood for the model to be sensitive to measurement noise. The reduced order model, in this case, is analogue to Equation (3.25) with the modification that a_3 and b_3 are removed.

The parameter vector estimate $\hat{\theta}$ is determined such that it minimises the squared error by aggregating the data series into a matrix ϕ:

$$\phi = [\varphi(4) \quad \cdots \quad \varphi(N)] \tag{3.28}$$

Consequently, the parameter vector estimate minimising the squared error, $\hat{\theta}_{LS}$, is found as

$$\hat{\theta}_{LS} = (\phi^T \phi)^{-1} \phi^T \mathbf{y} \tag{3.29}$$

or, in cases where ϕ is ill-conditioned, with the truncated least squares or truncated singular value decomposition (see e.g. [12]). The vector $\mathbf{y}$ is then

$$\mathbf{y} = [y(4) \quad \cdots \quad y(N)]^T \tag{3.30}$$

The estimated system $\hat{g}(q)$ is then, using the estimated parameters,

$$\hat{g}(q) = \frac{b_0 + b_1 q^{-1} + b_2 q^{-2} + b_3 q^{-3}}{1 + a_1 q^{-1} + a_2 q^{-2} + a_3 q^{-3}} \tag{3.31}$$

Modelling with recursive filter

Both the curve fitting disturbance removal and extended parametric model methods can be implemented in a recursive manner. By using an adaptive filter, as described in Section 2.1.8, continuous updates of the model parameters are determined, as new data becomes available. Barring the initialisation of the filter, the model always has a starting point for the parameter vector estimate $\hat{\theta}$, based on the last filter iteration, which can be assumed to be close to the minimum as the plants do not change much from sample to sample (10-15 minutes of adaptation to a change in background light was needed by Lindqvist [13] in order to avoid transient behaviour due to a change in stress level).

The model structure used for the recursive filter is the reduced order (two poles and two zeros) model described in Section 3.3.3.2. The filter is tested with initial parameters all set to 1 and with initial parameters equal to the ones calculated with the method described in Section 3.3.3.2. The forgetting factor α is chosen arbitrarily to 0.998 (see Figure 3.6), with a sampling time of 1 s, as it was considered to coincide somewhat with

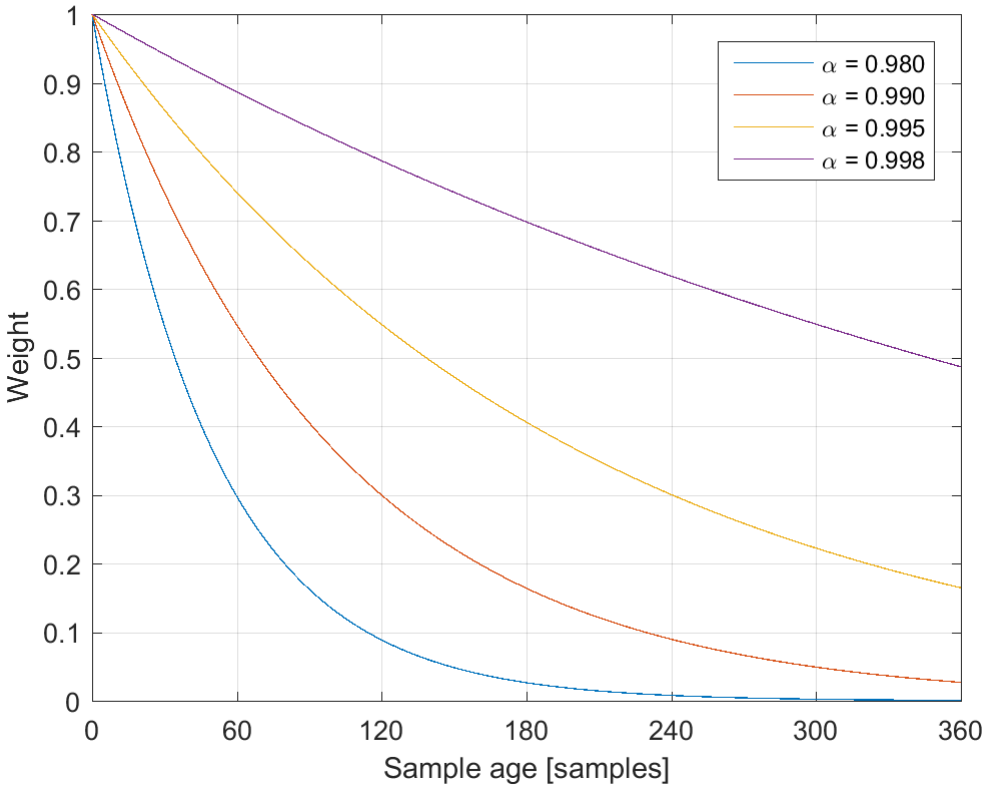

Figure 3.6: Weight on a sample resulting from different forgetting factors α, relating to how many samples ago the sample was taken. As the sampling time used is 1 s, the unit on the horizontal axis is also time.

the time scale at which plants react to external stress. For reference, field experiments with traditional ChlF excitation typically require a 30 minute relaxation period between two excitation flashes [16].

3.3.4 Simulation

In order to test the methods presented in Section 3.3.3, fluorescence data is generated using a known OE430 system, estimated from laboratory experiments on basil plants. A disturbance mimicking sunlight is generated as white noise filtered through a low-pass Butterworth filter with cut-off frequency $0.157\,\mathrm{rad\,s^{-1}}$, so as to approximate the variations of sunlight. To the sunlight signal a step input is added, simulating the lamp signal. The two signals are added together to create the input to the OE430 model. The total input can be seen in the top plot of Figure 3.7. The output of the reference OE430 system can be seen in the bottom plot of Figure 3.7.

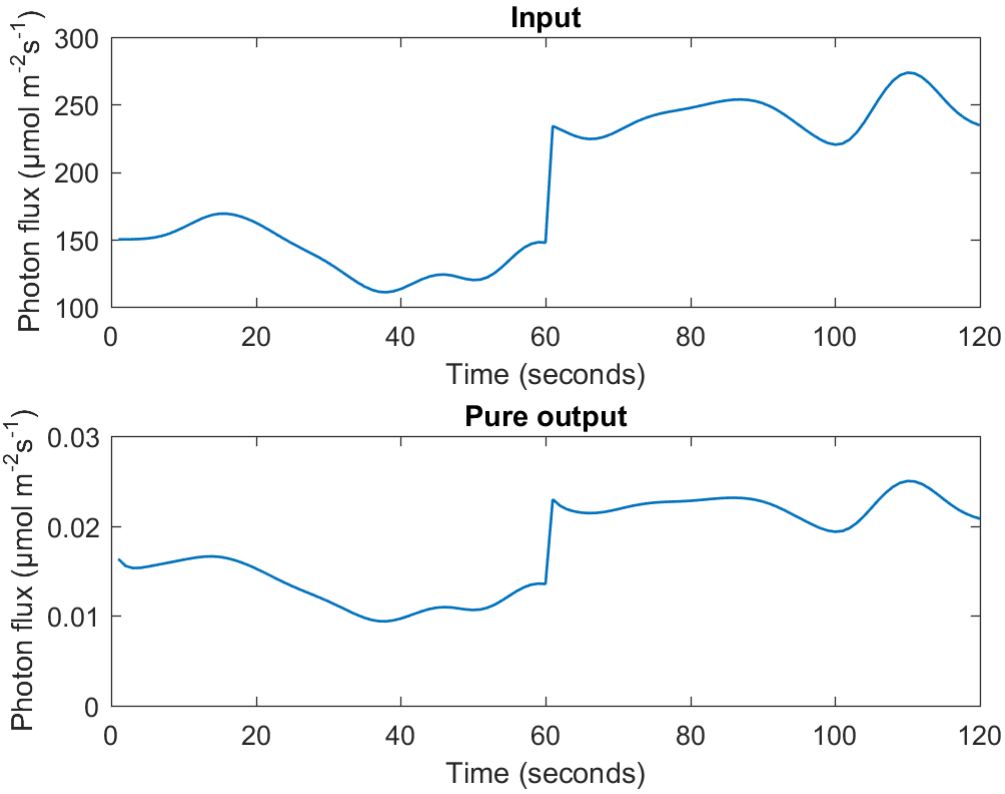

Figure 3.7: Input to and output from the reference OE430 system. The input is generated as filtered white noise, added with a step signal.

To accurately simulate the disturbing presence of sunlight, the output in Figure 3.7 is added with one or two more signals, creating two different tests. The first is to scale the sunlight signal and add it to the output, thus simulating reflection. The second also involves adding measurement noise, to test the sensitivity of the estimation algorithms used. The three signals are shown in Figure 3.8.

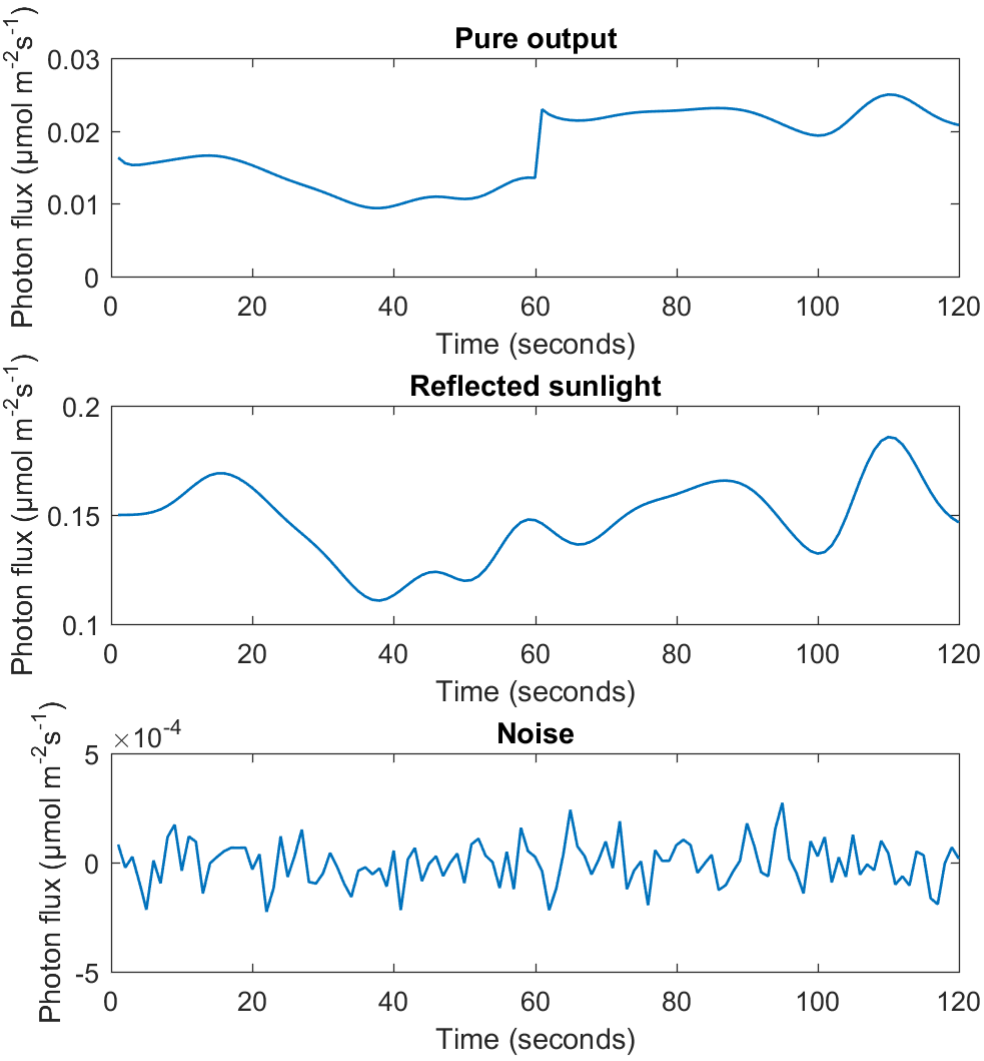

Figure 3.8: Composition of simulation signal. For the noise free test, the top two signals are added together to simulate reflection. The noise is then added to test the sensitivity to noise of the estimation algorithms used.

4

Results

Among the experiments conducted, six step responses are chosen to be displayed here. All six steps are taken from the April experiment, from a series of steps collected between 15:05 and 16:05 (the third of the step series described in Section 3.2.2). This measurement series is shown in Figure 4.7. Unfortunately, during this period, the light collected by the spectrometer facing the canopy is very different from the light collected by the spectrometer collecting sunlight (see especially Figure 4.11, bottom two plots, as compared to Figure 4.10). This is due to the vast difference in light environments measured by two spectrometers with different placement. Therefore, the interval from 850 nm to 1000 nm is used wherever possible (all cases except where FLD is used) to create the sunlight signal. The April experiment is chosen as it is the only one where a verification experiment has also been performed. Within the April experiment, the particular step series used in this chapter has been chosen as it is temporally close to the verification experiment. The fifth step series, while closer in time to the verification experiment, is not used as it is disturbed too much by reflections and shading from within the greenhouse. Details of the verification experiment can be found in Appendix B — only the resulting mean system is used here, shown in all Bode plots in black.

4.1 Method validation through simulation

Using the OE430 system known beforehand, input and output signals are generated as previously explained in Section 3.3.4. Based on this data, the signal processing methods of Section 3.3.3 are evaluated theoretically.

Firstly, curve fitting disturbance removal is tested on simulated data, with results shown in Figure 4.1 and Figure 4.2. A fit less than 100 % is expected as there is noise present.

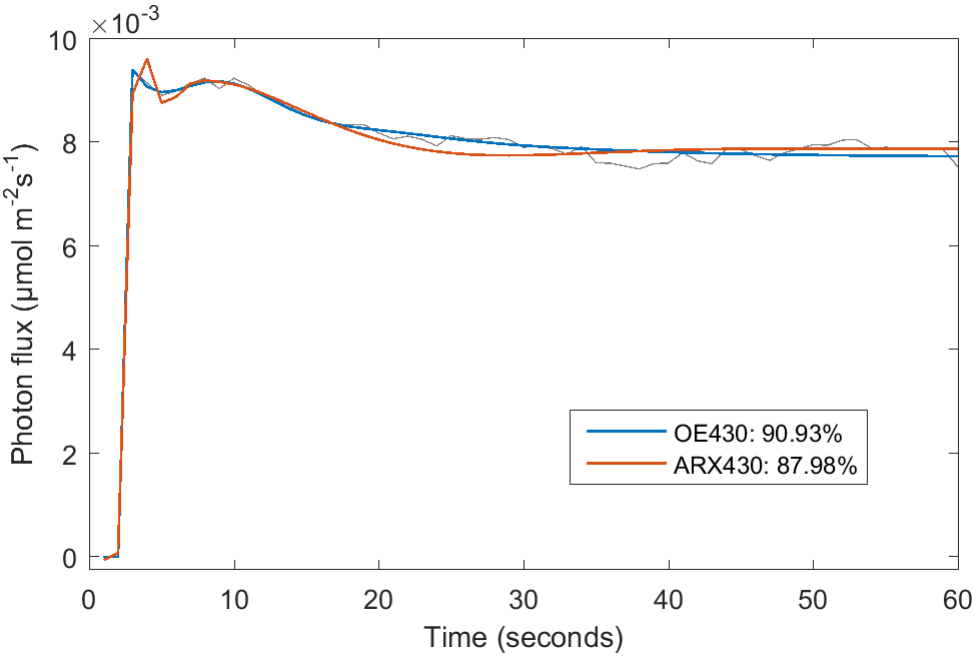

Figure 4.1: Simulation results of curve fitting disturbance removal. Two model structures are used to generate the output.

Both an OE and an ARX model are fitted to data, as the resulting error from the curve fitting method is likely to be of different character than measurement noise. Two model structures are used as the resulting error from the operation reasonably has different properties than measurement noise. The fit percentage is good considering the presence of noise, however it is clear that the ARX model is missing some characteristics of the true system.

Fitting the extended parametric model detailed in Section 3.3.3.2 to simulation data yields the result shown in Figure 4.3, with Bode diagram shown in Figure 4.4, for the noise free case. The estimated system is shown in blue. The least squares solution was found with singular value decomposition, and the Bode diagrams match perfectly.

In the case where noise is present, however, the situation is quite different. In order to arrive at the OE estimate, an iterative method was used. Both the result from this method and the least squares solution are shown in Figure 4.5 and the corresponding Bode diagram in Figure 4.6. Even though the simulated model output is very accurate, the Bode diagram fit is not. A general similarity is still present as seen in Figure 4.6. The model in Equation (3.25) was also solved for the exact parameters with MATLAB's nonlinear least squares solver [26], using several different starting points. Using the known correct parameters gave the correct solution, indicating that the model structure is correct. However, perturbing the initial parameter values slightly causes the solver to end up in one of several other local minima, with incorrect parameter values.

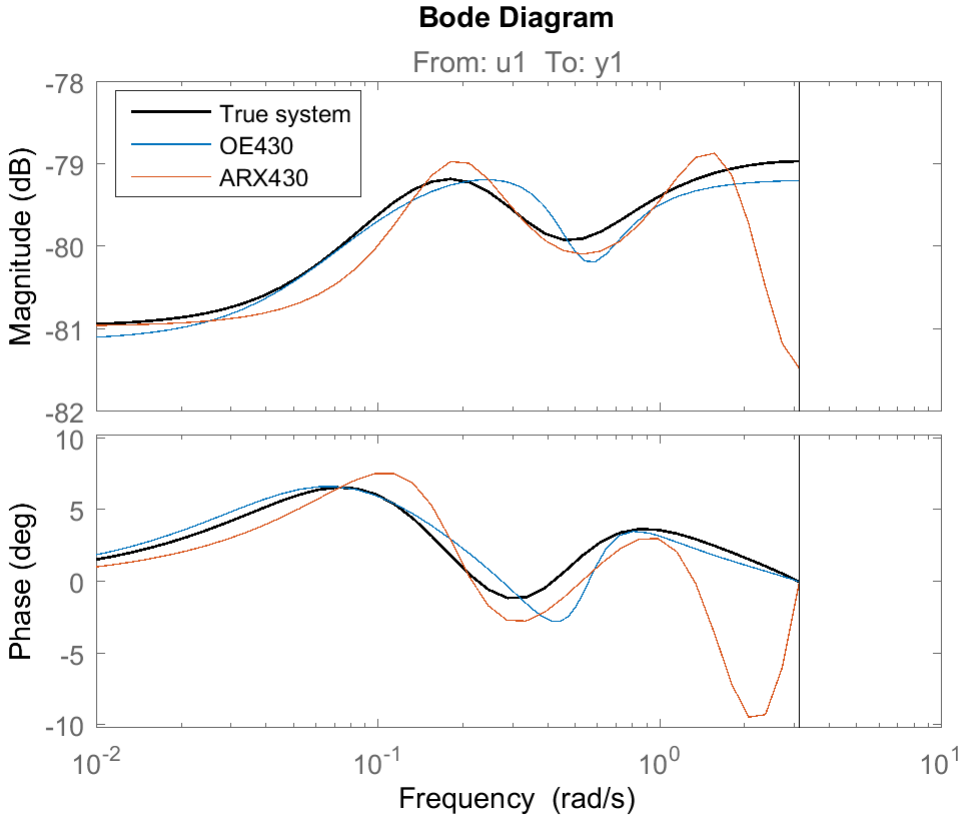

Figure 4.2: Bode diagrams of the estimated OE and ARX systems, using data where the disturbance has been removed with curve fitting, compared to the true system. The true system has been estimated as an OE system on laboratory ChlF measurement data.

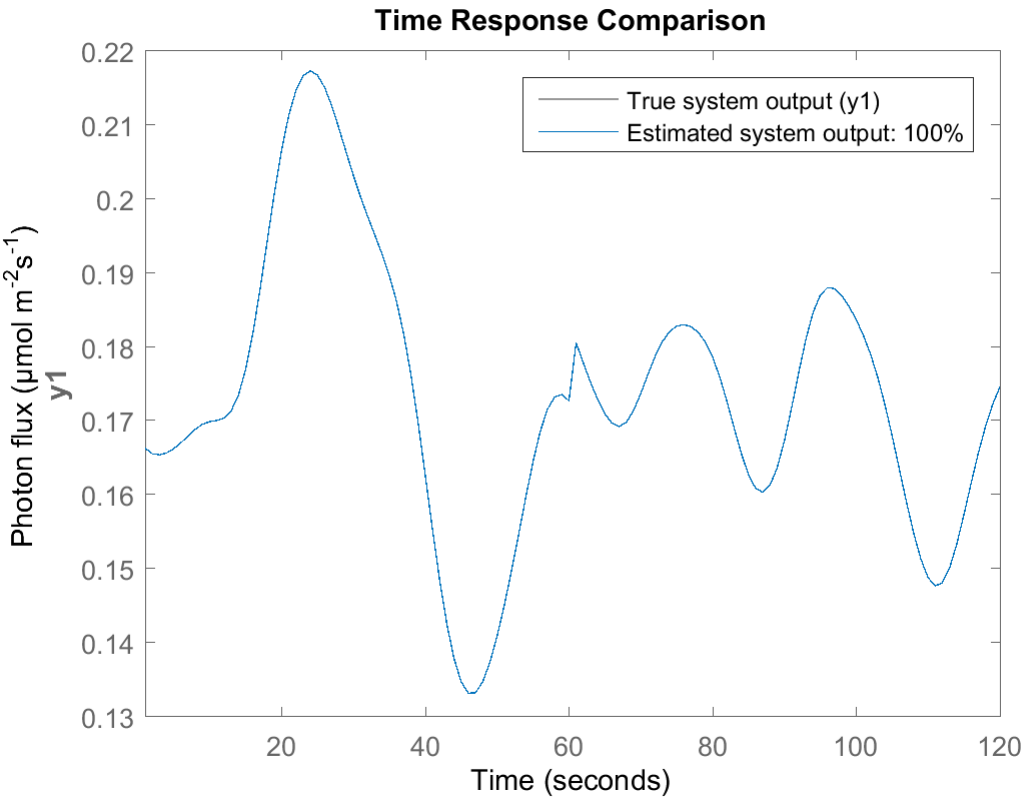

Figure 4.3: Output of the estimated model (blue) and the noise free data used to estimate the model (gray).

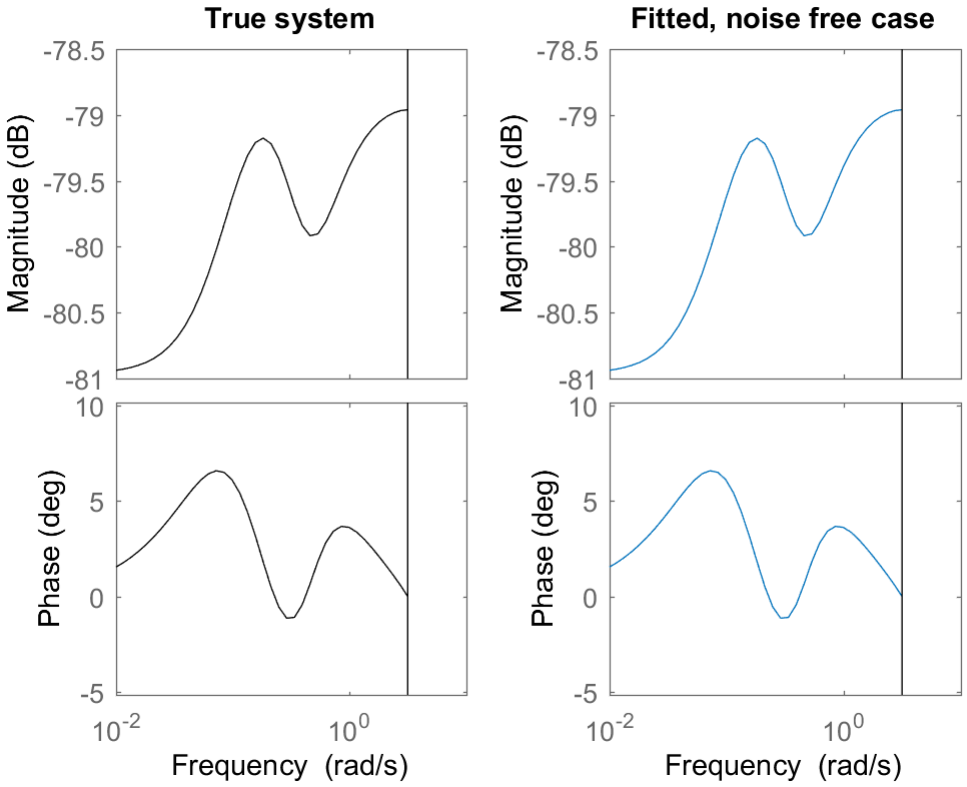

Figure 4.4: Bode diagram of the true system (left) and the estimated model (right). No noise is present in the estimation data, and therefore only the least squares solution is shown.

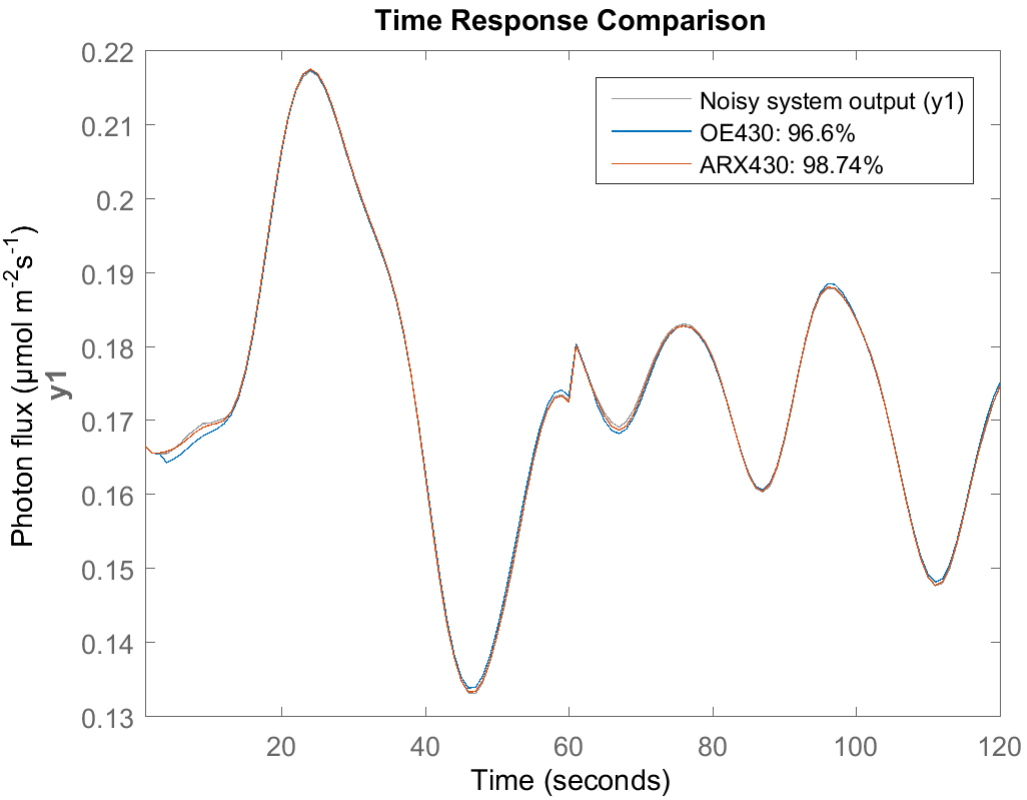

Figure 4.5: Output of the extended parametric model estimated with least squares (red), the iteratively refined model (blue) and the data corrupted by noise, used to estimate the model (gray).

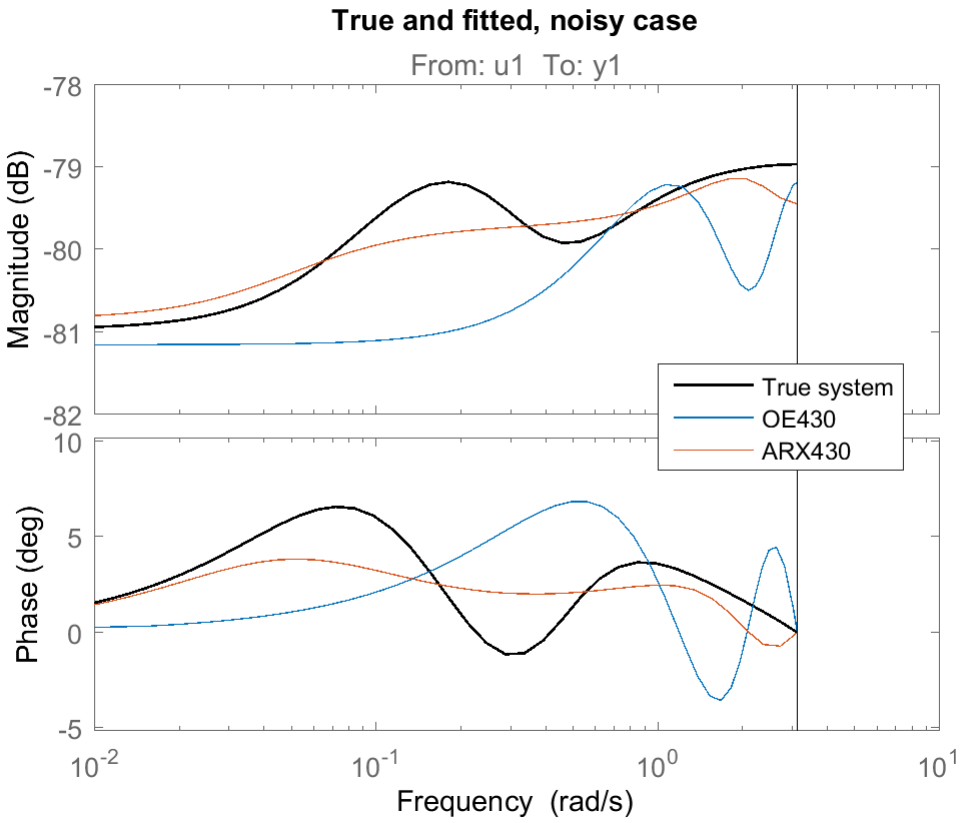

Figure 4.6: Bode diagram of the true system (black) along with the least squares model estimate (red), and the iteratively refined model (blue).

4.2 Experimental data

Figure 4.7 shows the entire experiment between 15:06 and 16:06. In the interest of brevity, six steps are chosen from this series: the 3rd, 6th, 14th, 24th, 27th and 28th steps. The selection is made at random, excluding those where the data had obviously been corrupted (such as the first step in Figure 4.7). Figure 4.8 to Figure 4.10 show the chosen

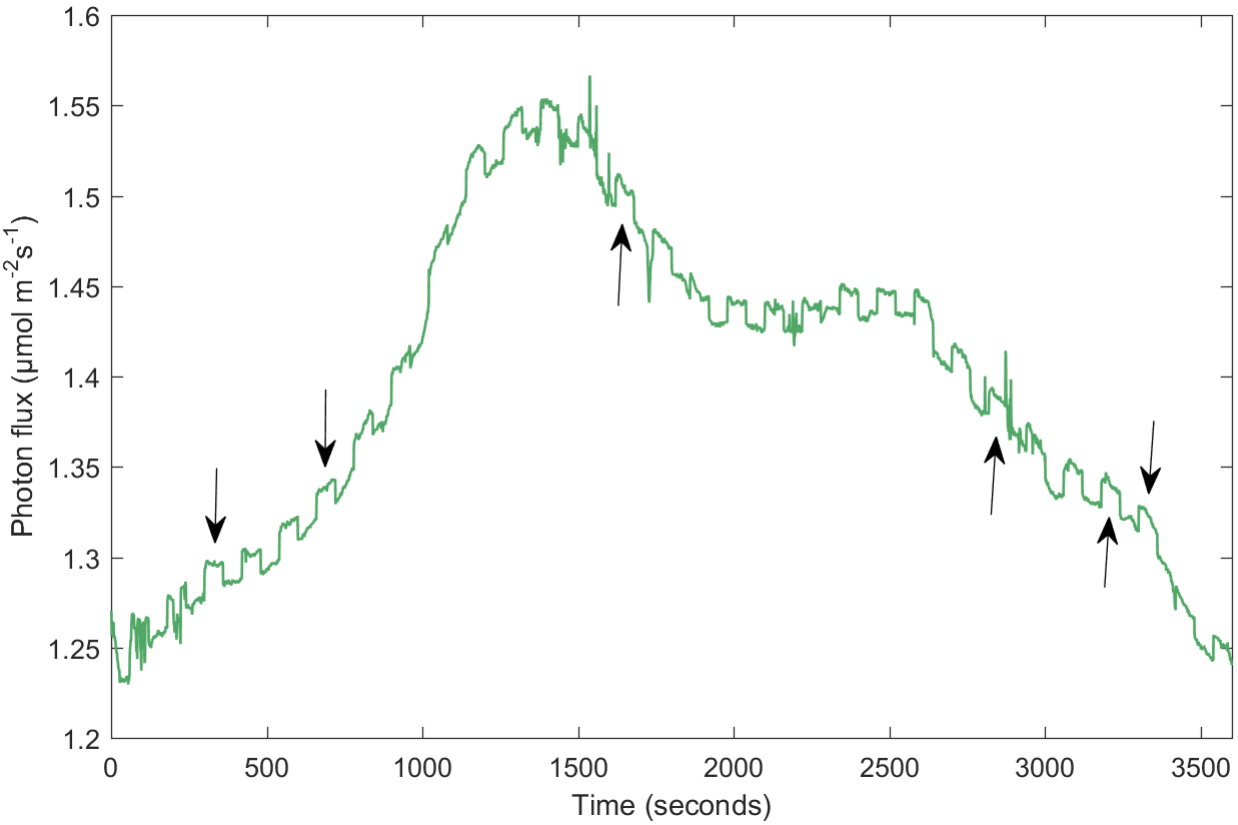

Figure 4.7: All 30 step responses, as measured by the spectrometer facing the canopy. The six steps which are used in this chapter are the 3rd, 6th, 14th, 24th, 27th and 28th steps in this figure. The data is integrated over the interval from 735 nm to 755 nm.

steps in more detail, as integrated over two different intervals (735 nm to 755 nm and 850 nm to 1000 nm, respectively). Figure 4.11 shows the sunlight as measured by the topmost spectrometer, integrated over the PAR interval. It is clear that the measured sunlight does not match the reflected which can be seen in Figures 4.8 - 4.10. This is due to the placement of the spectrometers. The bottom two plots are disturbed by shadows cast by structures in the greenhouse, and the measured light is therefore vastly different from the light reaching the plant canopy. Figure 4.12 shows the total incoming lamp

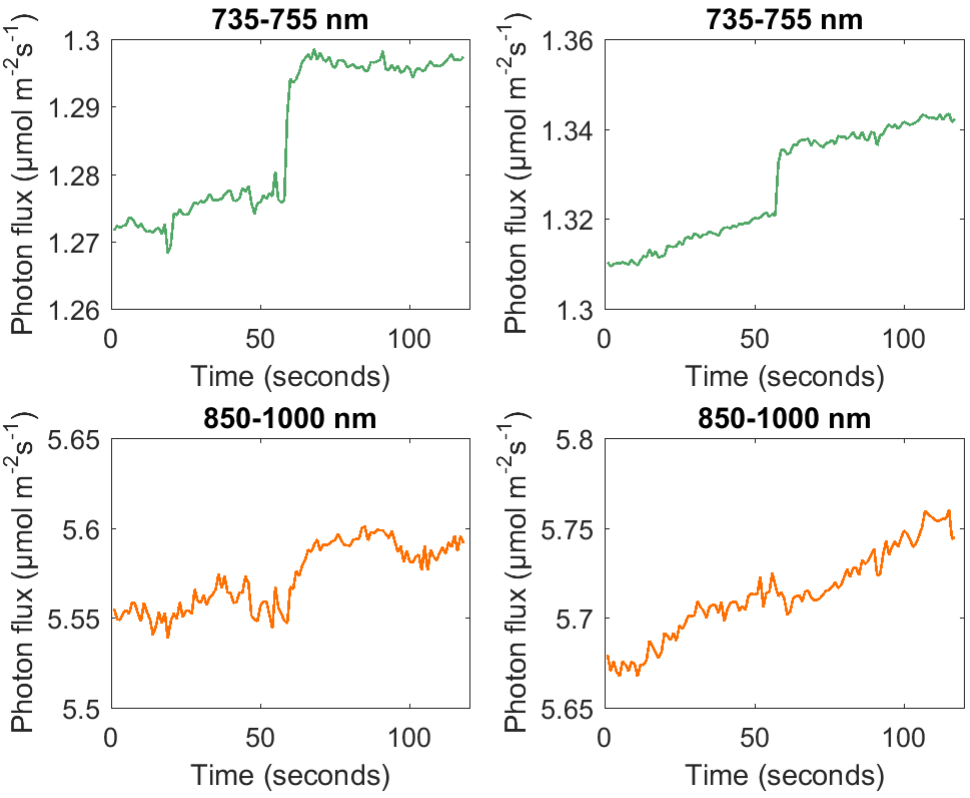

Figure 4.8: The first two step responses. The top two plots show the fluorescence response to one step excitation from the lamp, as well as reflected sunlight in the ChlF wavelength interval. The bottom two plots show the corresponding reflected sunlight in the neighbouring wavelength band between 850 nm and 1000 nm. All data is taken from the spectrometer facing the plant canopy.

light and sunlight, measured by the bottom spectrometer and integrated over the PAR interval.

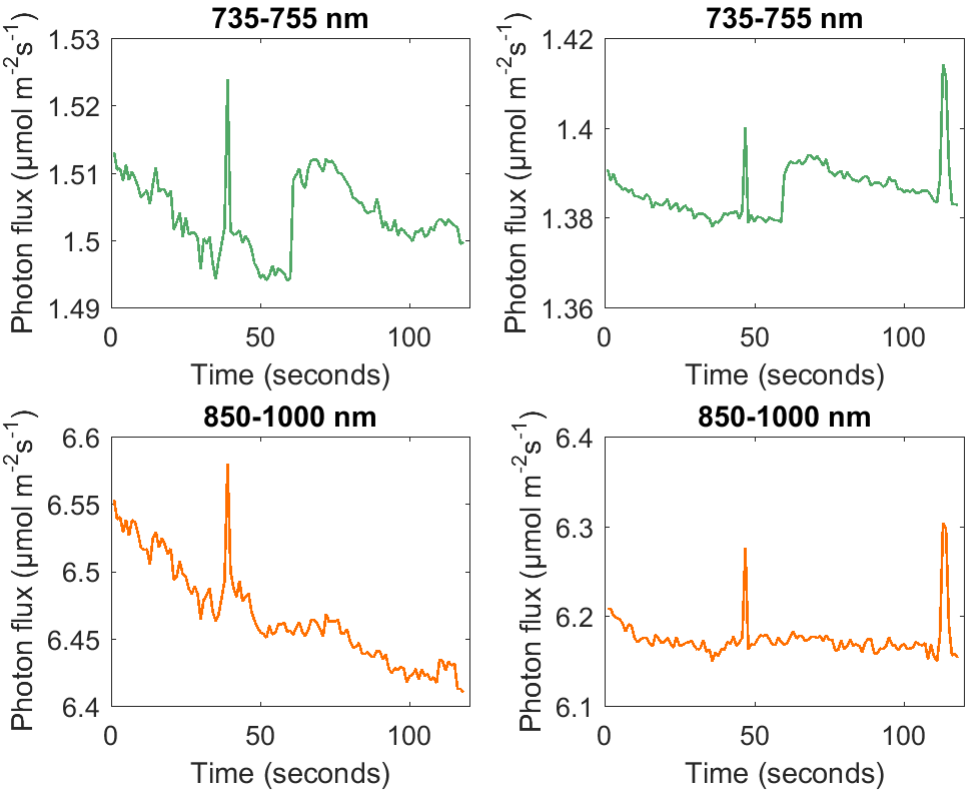

Figure 4.9: The third and fourth step responses. The top two plots show the fluorescence response to one step excitation from the lamp, as well as reflected sunlight in the ChlF wavelength interval. The bottom two plots show the corresponding reflected sunlight in the neighbouring wavelength band between 850 nm and 1000 nm. All data is taken from the spectrometer facing the plant canopy.

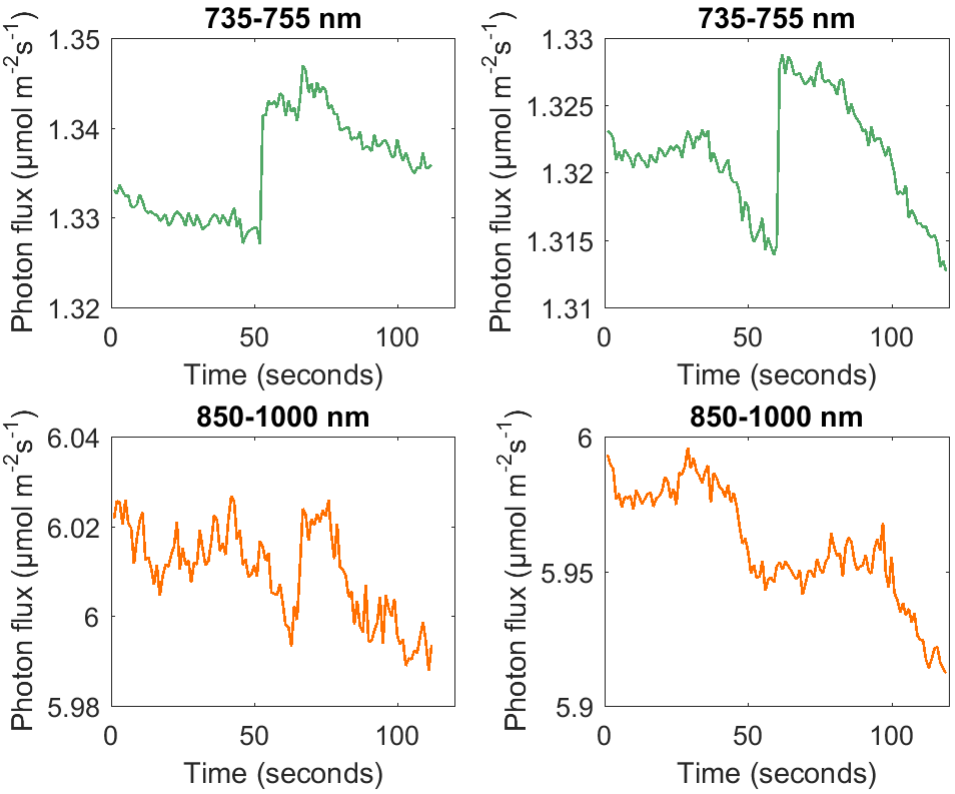

Figure 4.10: The fifth and sixth step responses. The top two plots show the fluorescence response to a step excitation from the lamp, as well as reflected sunlight in the ChlF wavelength interval. The bottom two plots show the corresponding reflected sunlight in the neighbouring wavelength band between 850 nm and 1000 nm. All data is taken from the spectrometer facing the plant canopy.

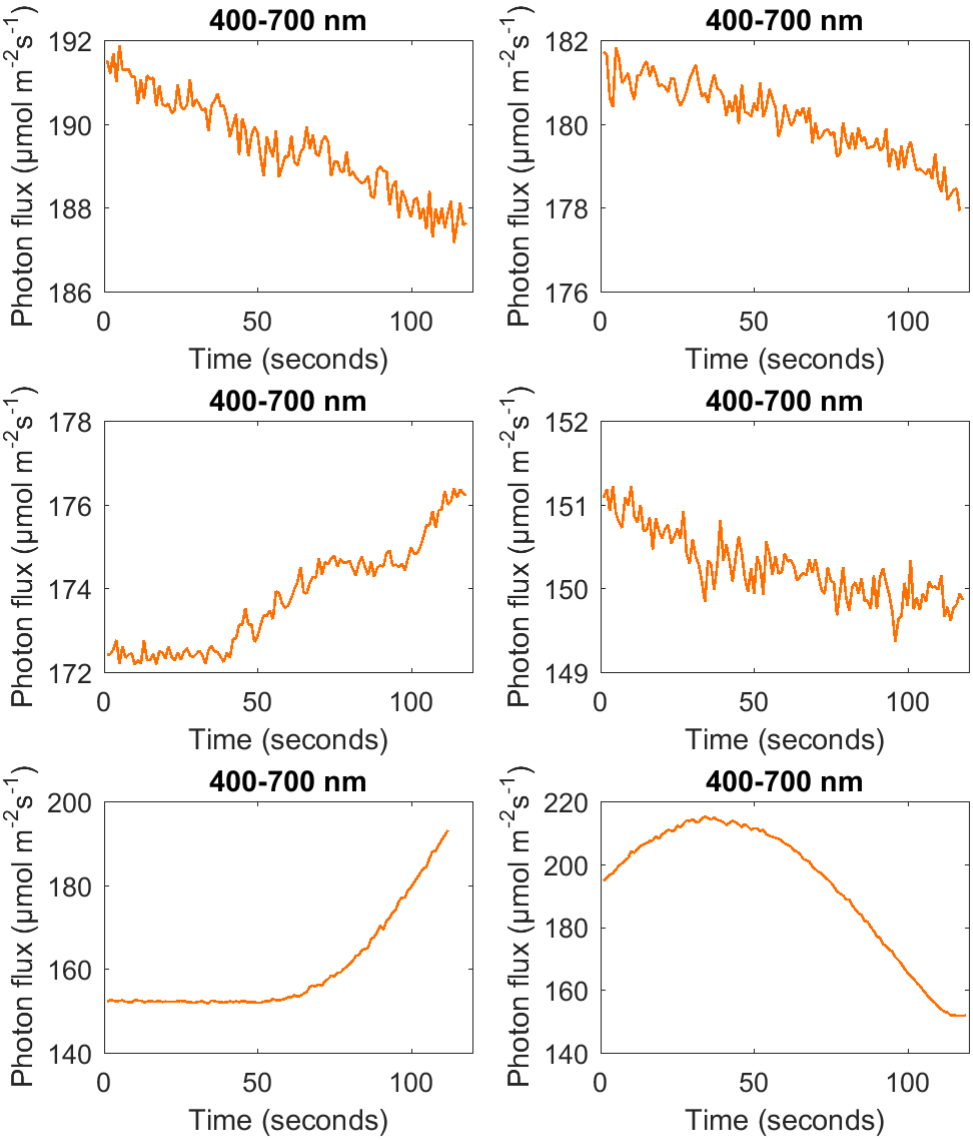

Figure 4.11: Sunlight during step excitations, as measured by the spectrometer collecting only sunlight.

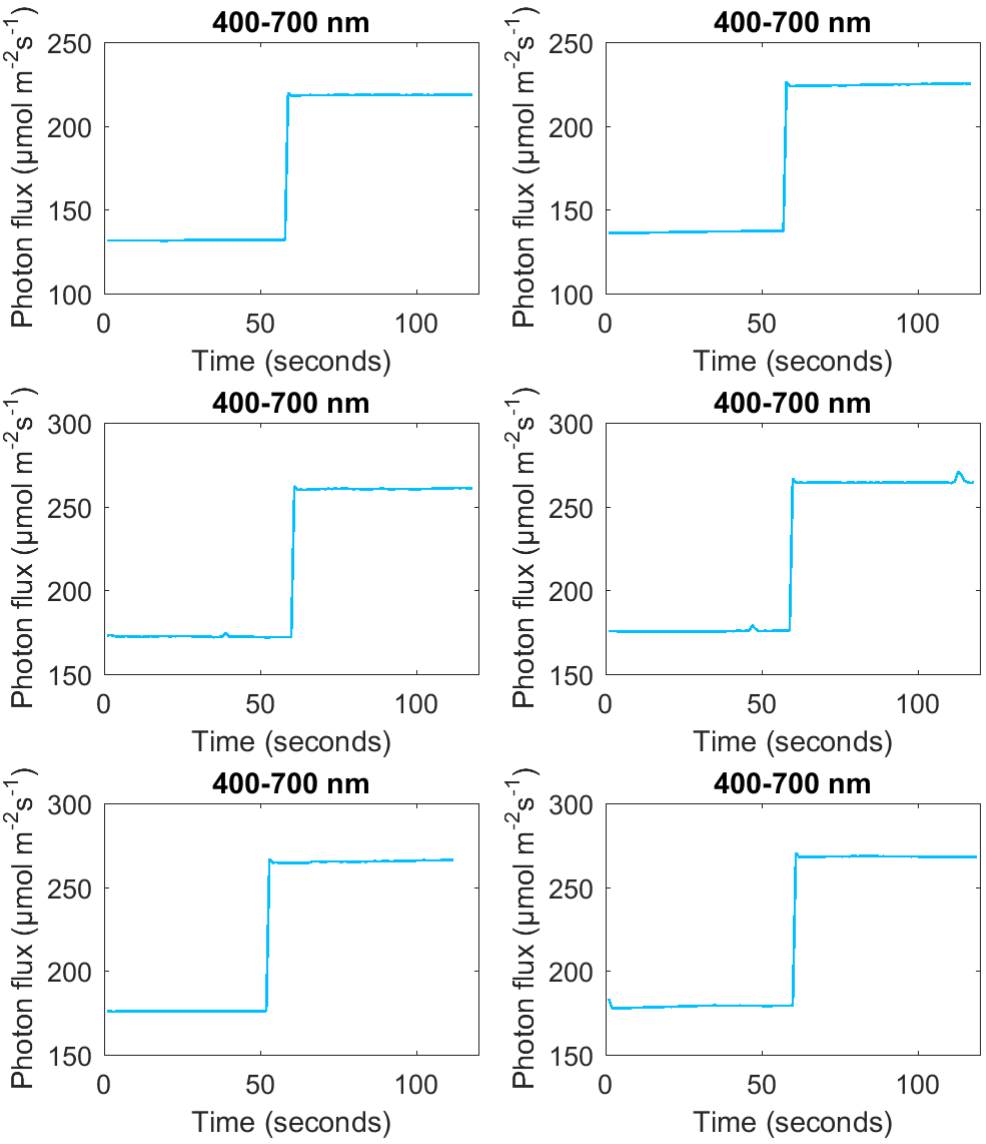

Figure 4.12: Measured total of incoming photosynthetically active lamp light and sunlight.

4.3 Method performance

Using the measurements shown in Section 4.2, the ChlF output is calculated using the methods detailed in Chapter 3. They are all clearly affected by measurement noise, to such a degree that the stress diagnosis becomes very unreliable. Further, it is not certain what character the ChlF response has when the plant canopy is affected by a varying background light level. The performance is evaluated as NRMSE fit percentage [27], in conjunction with similarity of the Bode diagram to the OE430 reference system. The reference system is estimated from data where the sun had no influence, but with a similar background level as provided by the sun. Furthermore, the reference experiment was performed directly following the experiment under influence of sunlight. Details on the reference experiment can be found in Appendix B.

The Bode diagrams in this section are all normalised to the gain at $0.01\,\mathrm{rad\,s^{-1}}$, as this is the lowest frequency of interest (approximately the steady-state gain), as described in [13]. Normalising the gain clarifies the ratio between resonance frequency and steady-state gain.

4.3.1 Fraunhofer line discrimination

Figure 4.13 shows the fluorescence calculated with the method described in Section 3.3.2.1. The fluorescence dynamics are somewhat visible. However, any high frequency content, such as an initial smaller peak, is likely to be lost in noise. OE320 models are fitted to the calculated ChlF responses, shown in Figure 4.14, as the higher order model structure has a tendency to model noise. The Bode diagrams of these systems are found in Figure 4.15.

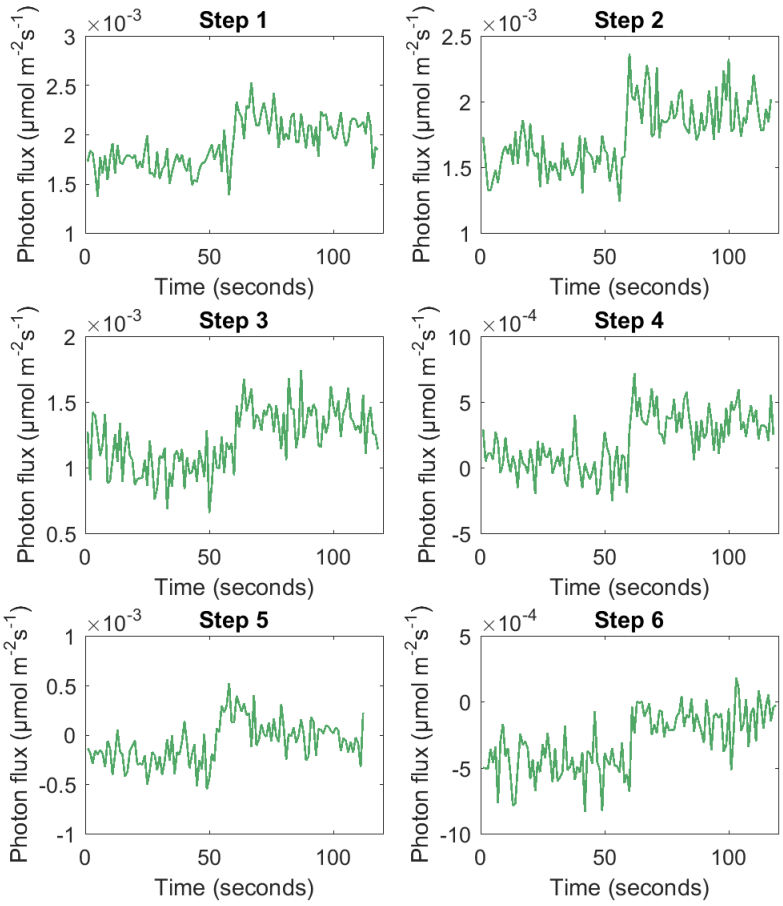

Figure 4.13: The six ChlF step responses, calculated with Fraunhofer line discrimination.

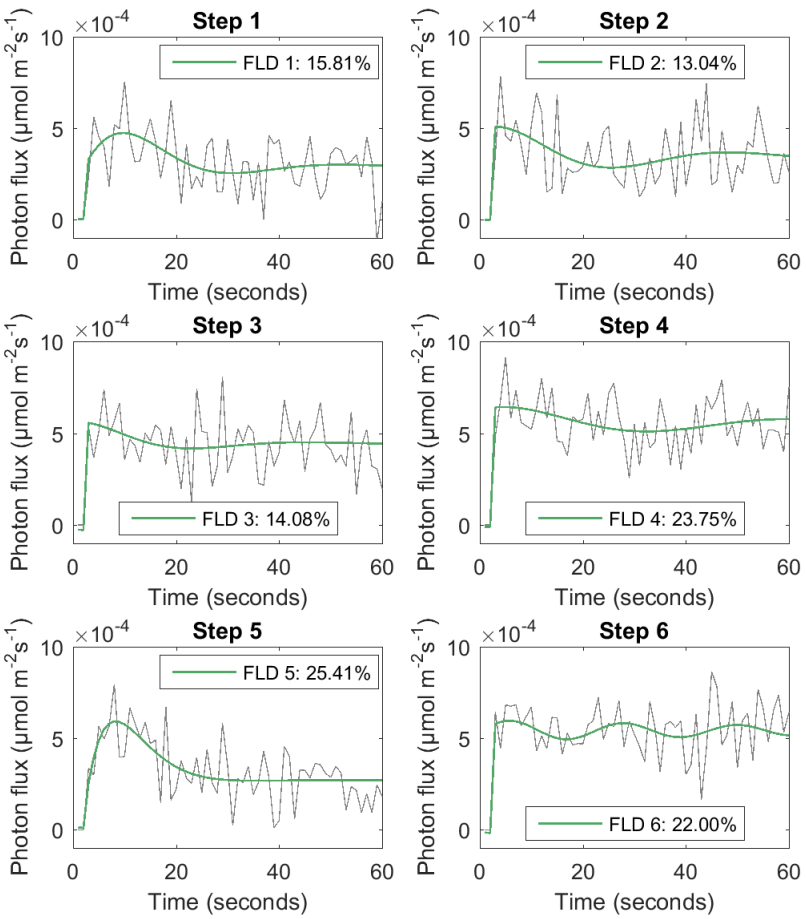

Figure 4.14: OE320 models fitted to the ChlF output calculated by means of Fraunhofer line discrimination.

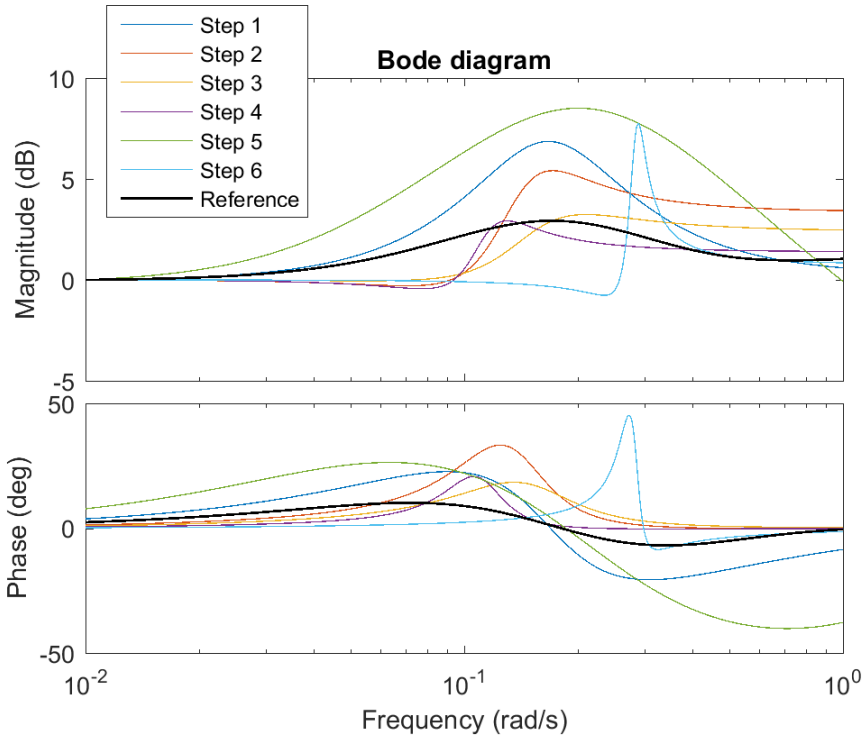

Figure 4.15: Bode diagrams of the OE320 models fitted to FLD output data. The reference system is shown as a thicker black line.

4.3.2 Curve fitting disturbance removal

Figure 4.16 shows the effect of fitting the sunlight signal to the fluorescence signal to remove the reflection, as described in Section 3.3.3.1. The plots shown are fluorescence data prior and post treatment with this method, as well as the sunlight signal being fitted.

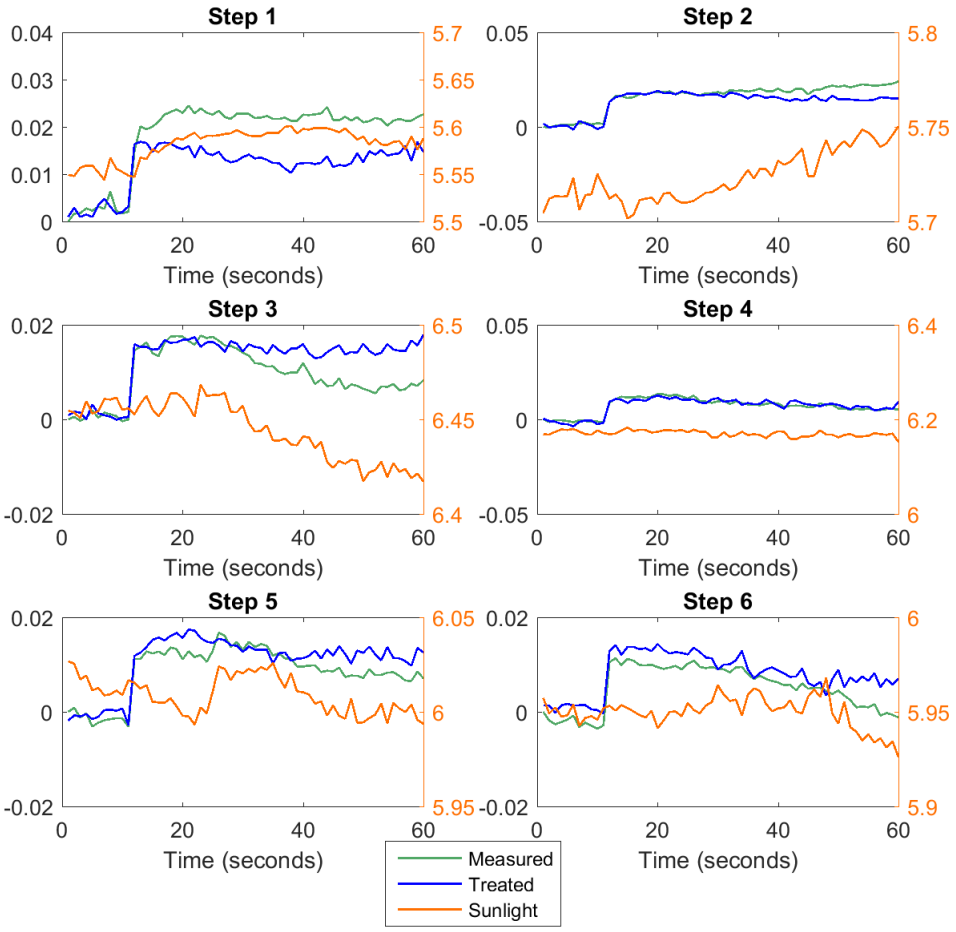

Figure 4.16: Performance of the curve fitting method. The sunlight is integrated over the interval 850 - 1000 nm for the canopy facing spectrometer. The sunlight is shown in orange (right axis). The fluorescence measured in the interval 735 - 755 nm is shown in green (left axis). It has been shifted down to fit into the plot. The signal resulting from the curve fitting is shown in blue (left axis).

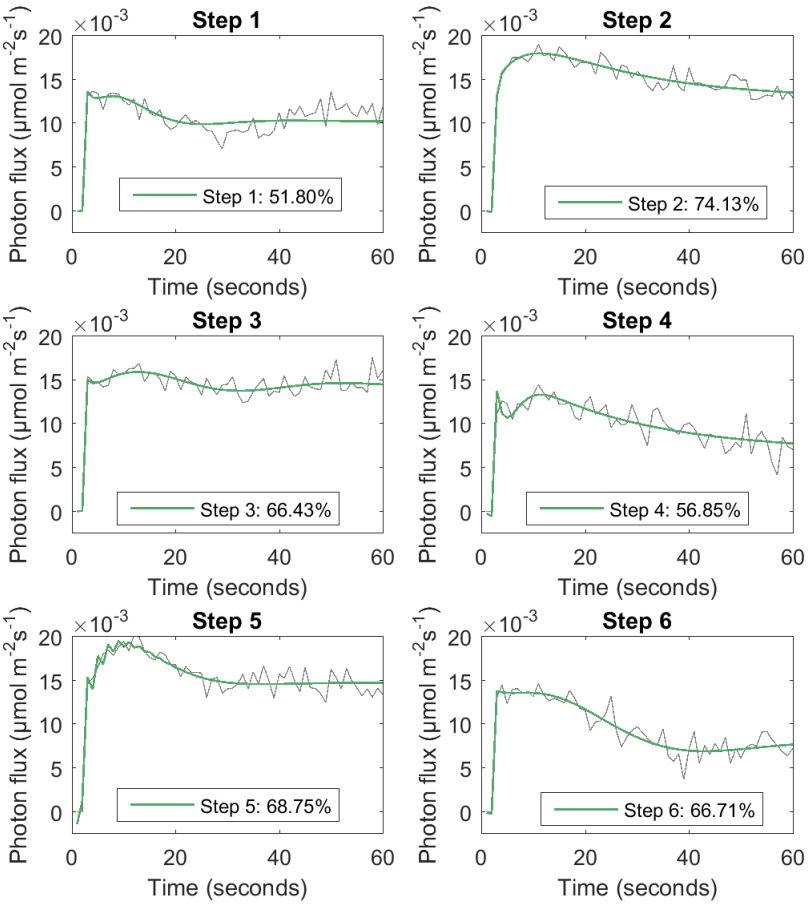

Figure 4.17: OE430 models fitted to the six different steps. The reflected sunlight has been removed from the output data (gray) through fitting of the sunlight signal to the raw irradiance data. All units are in $\mu\text{mol}\,\text{m}^{-2}\,\text{s}^{-1}$.

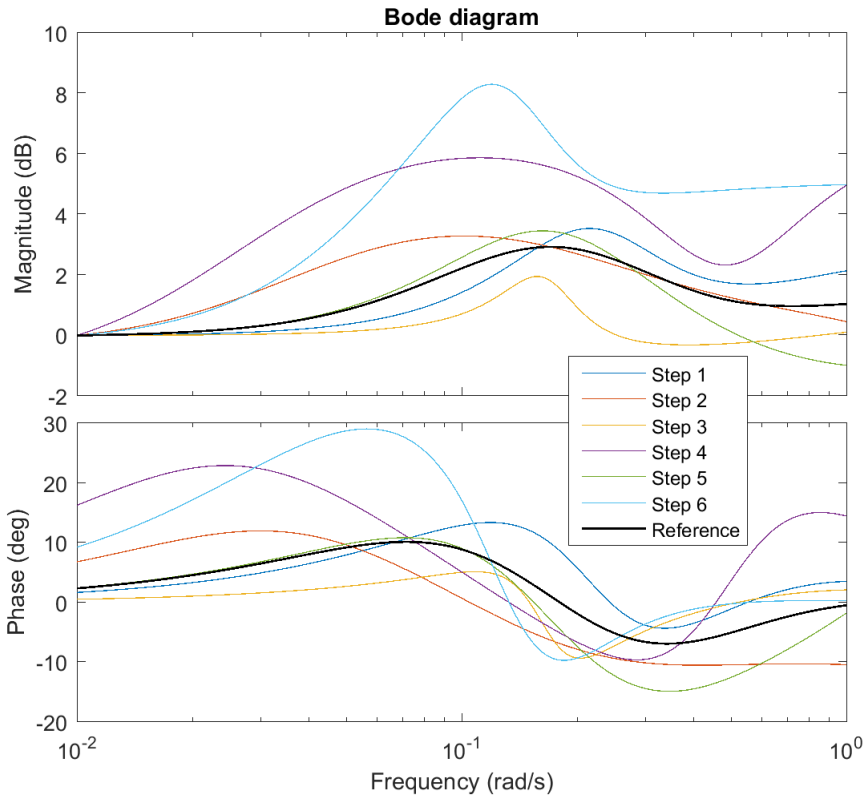

Figure 4.18: Bode diagrams of the six estimated OE430 systems, which are also shown in Figure 4.17. The systems are estimated from data treated by curve fitting disturbance removal. The reference system is shown as a thicker black line.

4.3.3 Spectral quotient

Figures 4.19 shows OE320 models fitted to experiment data where sunlight reflection and sunlight induced ChlF has been removed as described in Section 3.3.2.2. Figure 4.20 shows Bode diagrams for the estimated systems, as compared to the reference system.

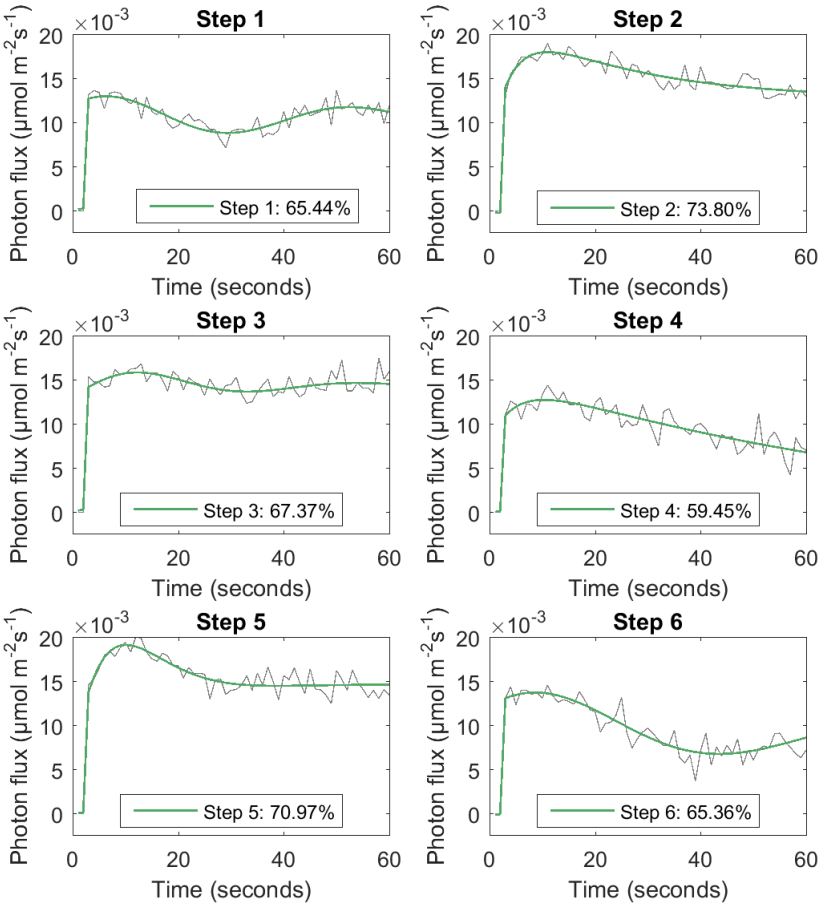

Figure 4.19: OE320 models fitted to the ChlF output calculated by means of spectral quotient.

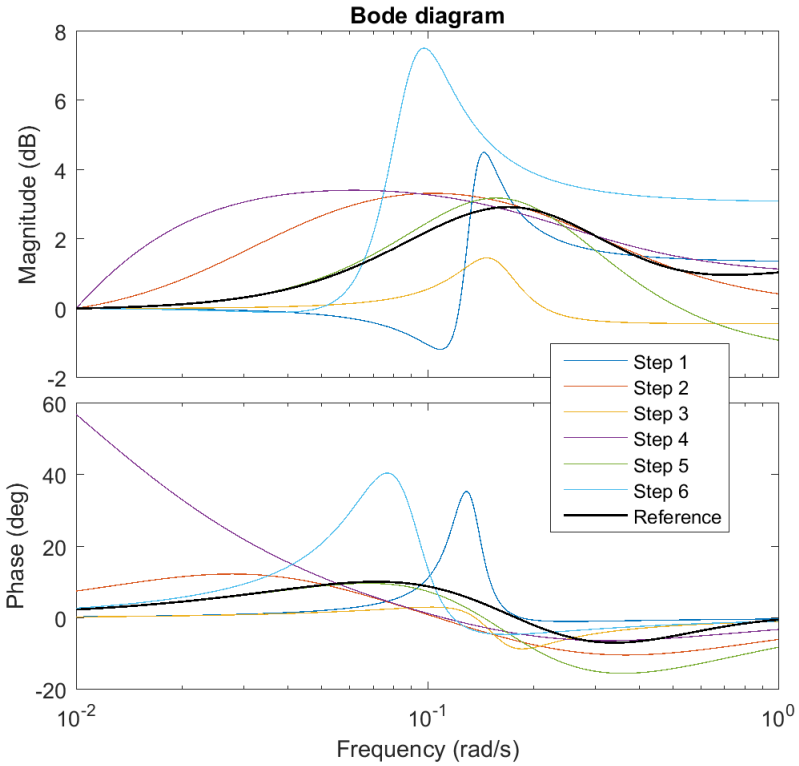

Figure 4.20: Bode diagrams of the OE320 models fitted to spectral quotient output data. Gains are normalised to the gain at $0.01\,\mathrm{rad\,s^{-1}}$. The reference system is shown as a thicker black line.

4.3.4 Parametric modelling

As the estimation of the parametric model in Equation (3.25) gives unsatisfactory results with simulation data, it is not expected to perform well with measured data. Nevertheless, the results are presented here, in Figure 4.21, Figure 4.22 and Figure 4.23. Figure 4.21 shows the model outputs when subjected to the measured input (sunlight and lamp light) data. The relatively low noise attenuation is likely due to the high feedthrough gain of the sunlight zero polynomial (reflectance). Figure 4.22 shows Bode diagrams of the fitted OE430 models, and Figure 4.23 shows Bode diagrams for the corresponding ARX430 models.

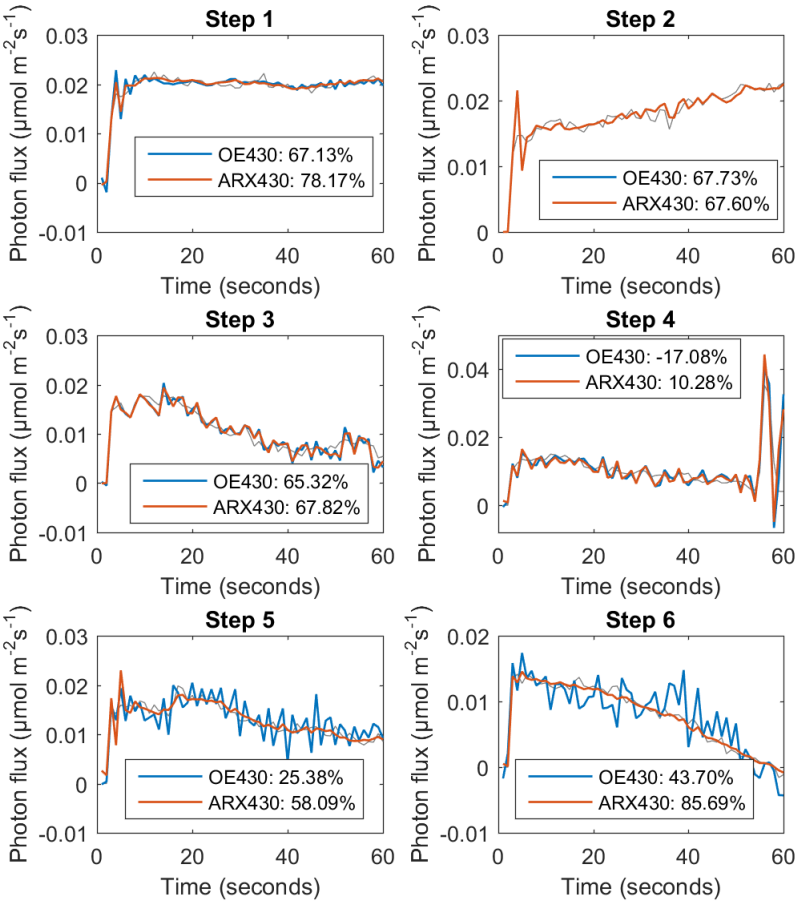

Figure 4.21: Extended ARX430 and OE430 models fitted to measurement data

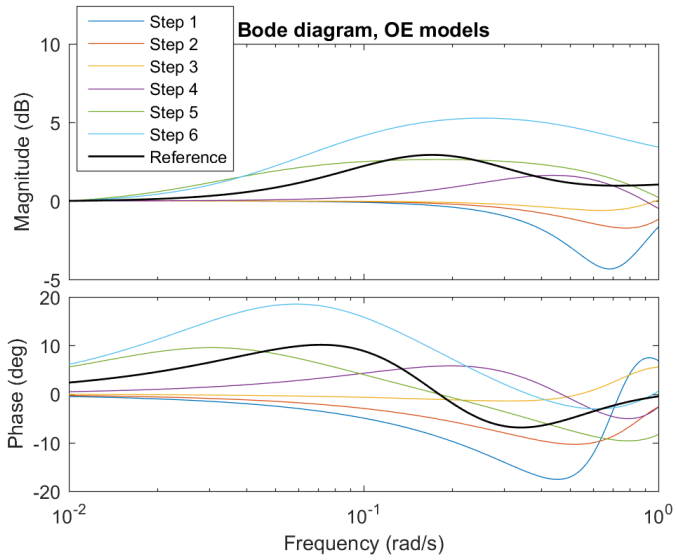

Figure 4.22: Bode diagrams for the extended OE430 model estimates. Gains are normalised to the gain at $0.01\,\mathrm{rad\,s^{-1}}$. The reference system is shown as a thicker black line.

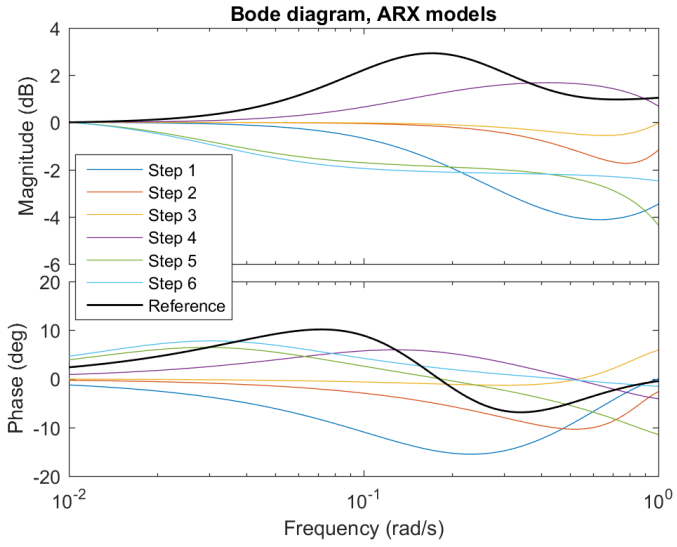

Figure 4.23: Bode diagrams for the extended ARX430 model estimates. Gains are normalised to the gain at $0.01\,\mathrm{rad\,s^{-1}}$. The reference system is shown as a thicker black line.

A singular value decomposition of the regressor matrix ϕ for one of the steps reveals the following singular values σ_i:

$$\{\sigma_1, ..., \sigma_{11}\} = \{1.700 \cdot 10^3,\ 1.453 \cdot 10^2,\ 8.375 \cdot 10^1,\ 7.804 \cdot 10^1,\ 6.036 \cdot 10^1,\ 6.067 \cdot 10^{-2},\ 4.734 \cdot 10^{-2},\ 4.494 \cdot 10^{-2},\ 2.433 \cdot 10^{-2},\ 8.745 \cdot 10^{-3},\ 7.331 \cdot 10^{-3}\} \tag{4.1}$$

The condition number of the matrix is very large, and the smallest singular value is small. This indicates that the matrix is (a) ill-conditioned and (b) close to losing rank. The problem of ill-conditioning is solved with regularisation by means of truncated singular value decomposition. The issue of rank is discussed further in Chapter 5.

4.3.5 Adaptive filtering

The results for the adaptive filter were not created for data where a verification experiment was made, due to accurate parameter estimation for the parametric model not being possible as shown by simulations.

5

Discussion

This study builds on and contributes to work in both spectrometry and chlorophyll fluorescence analysis. The main contribution of this study is combining remote sensing of ChlF responses with disturbance rejection techniques. In this chapter, the developed methods are discussed and an attempt at evaluation is made. Furthermore, some possible extensions of this work are suggested.

5.1 Methods

As the inner workings of the plant canopy is unknown to the outside observer, it is hard to know what the step responses should look like. To exemplify, studying Figure 4.7, which contains all steps, reveals that many of the steps do not have a typical ChlF step response appearance. It may be so that PSII reacts differently to a step under a changing background level, and that the identified systems therefore cannot be expected to be the same. Verification with simulation data is therefore a reasonable approach; if the canopy behaves differently under varying sunlight, that needs to be accounted for in a different manner (e.g. only performing step excitations under constant sunlight, though however, there should be better ways).

Furthermore, models with similar fit to the noisy data, i.e. similar fit percentages and appearance, can have widely different phase plots. In the case with noise, it is therefore unreliable to use the phase plot for stress diagnosis.

Aspects pertaining to the individual methods are discussed below.

5.1.1 Fraunhofer Line Discrimination

The modification of using least squares with the cFLD method laid forth by Gómez-Chova *et al.* [8] and Moya *et al.* [20], outlined in Section 3.3.2.1 ("modified assumptions"), aid considerably in extracting the fluorescence response from sunlight-contaminated signals. It is not certain why this has not been performed in other studies on ChlF in the presence of sunlight. Presumably, the increased accuracy of the results obtained is less clear when atmospheric modelling software and more accurate spectrometers are used (which is the case for all spectrometric studies referred to herein). Lack of atmospheric modelling software is most likely part of the reason why FLD does not remove all of the reflected sunlight - there is bound to be a small amount of path reflected radiance as well as an upwelling transmittance lower than 1. Furthermore, the spectral resolution of the spectrometers used causes a reduction in the absorption band depth. Thus, some light from adjacent wavelengths is included in the absorption band due to pixel quantisation in the spectrometer.

5.1.2 Spectral quotient

This method is, in essence, the same as the curve fitting approach, with the small exception that it only uses samples before the excitation step. The two are, however, formulated in two very different ways. It would be expected that using only the samples before the step would give performance in removing the sunlight, as the ChlF response to lamp light does not affect the 'fit'. The full curve fitting approach does however seem more effective at removing the reflected sunlight, when looking at the results.

5.1.3 Curve fitting disturbance removal

Removal of sunlight from the measured fluorescence signal by means of sunlight curve fitting as described in Section 3.3.3.1 is problematic. If the sunlight varies in a way similar to the fluorescence response it is highly probable that the sunlight curve is overly fitted to the response rather than the reflected sunlight. Furthermore, although less prevalent, this is the case also when the sunlight behaves benignly (i.e. not changing in a different way when the ChlF response is occurring). It should, however, be possible to weight the fit so that a good fit is less prioritised where ChlF can be expected - the problem, then, becomes how to shape the weighting so that it does not affect the fit negatively.

Theoretically, if the sunlight itself is not actinic, it should be possible to fit the sunlight curve only to where ChlF is not excited and hence avoid erringly fitting the curve to the response. The curve fitting method is better suited to static responses, and is essentially a very basic variant of the parametric model described by Equation (3.25) where only ρ is considered. The effect of using this method where a ChlF response is present is in

other words that $\hat{\rho}$ is overestimated, and that consequently some of the sunlight signal remains after the operation.

5.1.4 Parametric modelling

The extended model described by Equation (3.25) likely needs modification to be consistently solvable for the correct minimum. The slightest presence of noise using the current model iteration makes the solution unreliable for the purpose of stress diagnosis. Another candidate for why the model does not give reliable parameter values could be the observability or identifiability of the system. With the output $y(n)$ essentially being generated by two separate subsystems, the individual outputs of which it is not possible to know, it becomes difficult to know which of the two subsystems generates which part of the output.

A few of the small singular values in the regressor matrix ϕ are likely due to the matrix being Toeplitz structured (the same elements appear in block diagonals). However, the number of singular values which are exactly zero when noise is not present is only one. For the case with noise, this indicates that only one singular value is small due to this fact. The remaining small singular values are then due to near linear dependency between columns. This means that a parameter in θ can be estimated wrongly, and then compensated for in the fit by another parameter being estimated wrongly 'in the other direction'.

The fact that noise is present in the regressor matrix ϕ, both in input and output values, makes the least squares solution biased. While the instrumental variable method is used to iteratively improve this solution, the method does not handle input noise well.

If a personal evaluation is to be given, this method appears the most elegant; all of the other methods have some assumption worked into them. If it would be possible to estimate the parameters in this model in a consistent way, that would be the paramount solution to the DFRA-in-sunlight problem.

5.1.5 Adaptive filtering

The filter performance depends on the model structure being correct, and an evaluation of this approach is difficult to make as the approach could be spot on while it is the model structure that needs revision.

This method enables continuous monitoring and parameter updates; it would be an interesting experiment to use this method on a plant canopy which is subjected to a change in stress during the course of an experiment.

5.2 Future work

This section has been redacted from the published version of this text at the request of Heliospectra. It is available at the discretion of Heliospectra and the author.

6

Conclusion

Sunlight adversely affects the DFRA model estimation. If the sunlight is not constant, it continuously generates a ChlF response which disturbs the DFRA modelling. Furthermore, the feedthrough magnification of the estimated system is severely changed when some of the incoming light is merely reflected back instead of going through PSII to be output as ChlF. If the method is to be used with a changing background level, additional steps must be taken.

With the resolution of the spectrometers used in this work, the FLD method produces too much noise, however if higher resolution spectrometers were to be used (i.e. better than 1 nm) this method would likely give the best ChlF estimations. The output data from FLD can then be used directly in DFRA, if the input signal is taken to be both sunlight and lamp light. A negative aspect of this method is that it requires two spectrometers.

In contrast, using only one spectrometer to measure ChlF on the canopy, while simultaneously deducing the sunlight from reflected irradiance in the 850 - 1000 nm, proved to be a most successful approach. It lessens the noise arising from spectrometer integration times and requires only one spectrometer. If the intensity of the lamps at canopy level is known (which is not unlikely), this is the only spectrometer needed. However, this approach can only be used for the signal processing methods, which all have their own small problem.

The curve fitting disturbance removal method does not remove all sunlight, as the sunlight curve is partly fitted to the ChlF response to the lamp input. The extended parametric model estimation is the most elegant solution, however the problem is non-linear and difficult to solve for the correct parameter values, especially in the presence of noise. The adaptive filter is based upon the model and is in all likelihood a good approach however it is based on the model.

The DFRA method as a whole is sensitive to the non-linearity of the system, as the non-linear ChlF response dynamics is modelled as a linear system. While this is not a problem in laboratory conditions, the model mismatch is perfectly evident when there is a varying background disturbance. The fact that the system cannot be expected to react similarly to the same input signal makes even visual assessment of the response curves difficult.

With regard to the DFRA method in presence of noise, the phase plot is too sensitive with the present noise level, as it is not clear which model fit is better between two very similar fits. The models, which are similar in fit, can have a large difference in phase plots. It is therefore unreliable for showing plant stress in exposed environments, unless the noise is reduced by a considerable amount. Instead, it would be better to use the steady-state to resonance frequency gain ratio to diagnose plant stress, if the noise level cannot be reduced.

The most promising method for future applications is the adaptive filter, as it is better suited for automating plant stress detection, however it requires that model parameter estimation be solved in some way. If this cannot be done, FLD should be used in conjunction with precise spectrometers and shorter sampling time to combat the noise created by the method.

Bibliography

[1] L. Alonso, L. Gomez-Chova, J. Vila-Frances, J. Amoros-Lopez, L. Guanter, J. Calpe, and J. Moreno, "Improved fraunhofer line discrimination method for vegetation fluorescence quantification," *IEEE Geoscience and Remote Sensing Letters*, vol. 5, no. 4, pp. 620–624, 2008.

[2] A. Berk, G. P. Anderson, P. K. Acharya, L. S. Bernstein, L. Muratov, J. Lee, M. Fox, S. M. Adler-Golden, J. H. Chetwynd, M. L. Hoke, R. B. Lockwood, J. A. Gardner, T. W. Cooley, C. C. Borel, and P. E. Lewis, "Modtran 5: a reformulated atmospheric band model with auxiliary species and practical multiple scattering options: update," in *Proceedings of SPIE*, vol. 5806, 2005, pp. 662–667.

[3] C. Buschmann, "Variability and application of the chlorophyll fluorescence emission ratio red/far-red of leaves," *Photosynthesis Research*, vol. 92, no. 2, pp. 261–271, 2007.

[4] S. Butterworth, "On the theory of filter amplifiers," *Experimental wireless and the wireless engineer*, vol. 7, pp. 536–541, 1930.

[5] A.-M. Carstensen, T. Wik, and T. Pocock, "Remote light stress detection for greenhouse led lighting control," in *Proceedings 19th Nordic Process Control Workshop*, 2015, pp. 20:1–6.

[6] A.-M. Carstensen, T. Pocock, D. Bånkestad, and T. Wik, "Remote detection of light tolerance in basil through frequency and transient analysis of light induced fluorescence," *Computers and Electronics in Agriculture*, vol. 126, pp. 289–301, 2016.

[7] A.-M. Carstensen, T. Wik, D. Bånkestad, and T. Pocock, "Exploring the dynamics of remotely detected fluorescence transients from basil as a potential feedback for lighting control in greenhouses," *Acta Horticulturae*, vol. 1134, pp. 375–383, 2016.

[8] L. Gómez-Chova, L. Alonso, J. Amorós-López, J. Vila-Francés, S. del Valle-Tascón, J. Calpe, and J. Moreno, "Solar induced fluorescence measurements using a field

spectroradiometer," in *AIP Conference Proceedings*, vol. 852, no. 1, 2006, pp. 274–281.

[9] L. Guanter, L. Alonso, L. Gómez-Chova, M. Meroni, R. Preusker, J. Fischer, and J. Moreno, "Developments for vegetation fluorescence retrieval from spaceborne high-resolution spectrometry in the O_2-A and O_2-B absorption bands," *Journal of Geophysical Research: Atmospheres*, vol. 115, no. 19, 2010.

[10] T. Julitta, L. Corp, M. Rossini, A. Burkart, S. Cogliati, N. Davies, M. Hom, A. MacArthur, E. Middleton, U. Rascher, A. Schickling, and R. Colombo, "Comparison of sun-induced chlorophyll fluprescence estimates obtained from four portable field spectroradiometers," *Remote Sensing*, vol. 8, p. 122, 2014.

[11] Y. J. Kaufman and C. Sendra, "Algorithm for automatic atmospheric corrections to visible and near-ir satellite imagery," *International Journal of Remote Sensing*, vol. 9, no. 8, pp. 1357–1381, 1988.

[12] K. J. Keesman, *System identification: an introduction.* Springer, 2011.

[13] J. Lindqvist, "Remote detection of plant stress by analysis of the dynamic behaviour of chlorophyll a fluorescence response," Master's thesis, Chalmers University of Technology, Göteborg, 2015, institutionen för signaler och system, Chalmers tekniska högskola, nr: EX030/2015.

[14] L. Ljung and T. Glad, *Modeling of Dynamic Systems.* Prentice Hall, 1994.

[15] S. W. Maier, K. P. Günther, and M. Stellmes, "Sun-induced fluorescence: A new tool for precision farming," in *American Society of Agronomy Special Publication*, ser. Digital Imaging and Spectral Techniques: Applications to Precision Agriculture and Crop Physiology, 2003, vol. 66, pp. 209–222.

[16] K. Maxwell and G. N. Johnson, "Chlorophyll fluorescence - a practical guide," *Journal of Experimental Botany*, vol. 51, no. 345, pp. 659–668, 2000.

[17] K. McCree, "The action spectrum, absorptance and quantum yield of photosynthesis in crop plants," *Agricultural Meteorology*, vol. 852, no. 1, pp. 274–281, 1972.

[18] M. Meroni and R. Colombo, "Leaf level detection of solar induced chlorophyll fluorescence by means of a subnanometer resolution spectroradiometer," *Remote Sensing of Environment*, vol. 103, no. 4, pp. 438–448, 2006.

[19] M. Meroni, M. Rossini, L. Guanter, L. Alonso, U. Rascher, R. Colombo, and J. Moreno, "Remote sensing of solar-induced chlorophyll fluorescence: Review of methods and applications," *Remote Sensing of Environment*, vol. 113, no. 10, pp. 2037–2051, 2009.

[20] I. Moya, F. Daumard, A. Ounis, N. Moise, and Y. Goulas, "First airborne multiwavelength passive chlorophyll fluorescence measurements over La Mancha (Spain) fields," in *Proceedings of the 2nd international symposium on recent advances in quantitative remote sensing*, 2006, pp. 820–825.

[21] B. Mulgrew, P. Grant, and J. Thompson, *Digital signal processing - concepts and applications*. Palgrave Macmillan, 2003.

[22] J. Plascyk and F. Gabriel, "The fraunhofer line discriminator MKII - an airborne instrument for precise and standardized ecological luminescence measurement," in *IEEE Transactions on Instrumentation and Measurement*, vol. 24, no. 4, 1975, pp. 306–313.

[23] U. Rascher, G. Agati, L. Alonso, G. Cecchi, S. Champagne, R. Colombo, A. Damm, F. Daumard, E. de Miguel, G. Fernandez, B. Franch, J. Franke, C. Gerbig, B. Gioli, J. Gómez, Y. Goulas, L. Guanter, . Gutiérrez-de-la Cámara, K. Hamdi, P. Hostert, M. Jiménez, M. Kosvancova, D. Lognoli, M. Meroni, F. Miglietta, A. Moersch, J. Moreno, I. Moya, B. Neininger, A. Okujeni, A. Ounis, L. Palombi, V. Raimondi, A. Schickling, J. Sobrino, M. Stellmes, G. Toci, P. Toscano, T. Udelhoven, S. van der Linden, and A. Zaldei, "Cefles2: the remote sensing component to quantify photosynthetic efficiency from the leaf to the region by measuring sun-induced fluorescence in the oxygen absorption bands," *Biogeosciences*, vol. 6, pp. 1181–1198, 2009.

[24] U. Rascher, L. Alonso, A. Burkart, C. Cilia, S. Cogliati, R. Colombo, A. Damm, M. Drusch, L. Guanter, J. Hanus, T. Hyvärinen, T. Julitta, J. Jussila, K. Kataja, P. Kokkalis, S. Kraft, T. Kraska, M. Matveeva, J. Moreno, O. Muller, C. Panigada, M. Pikl, F. Pinto, L. Prey, R. Pude, M. Rossini, A. Schickling, U. Schurr, D. Schüttemeyer, J. Verrelst, and F. Zemek, "Sun-induced fluorescence – a new probe of photosynthesis: First maps from the imaging spectrometer HyPlant," *Global Change Biology*, vol. 21, no. 12, pp. 4673–4684, 2015.

[25] M. Rossini, L. Nedbal, L. Guanter, A. Ač, L. Alonso, A. Burkart, S. Cogliati, R. Colombo, A. Damm, M. Drusch, J. Hanus, R. Janoutova, T. Julitta, P. Kokkalis, J. Moreno, J. Novotny, C. Panigada, F. Pinto, A. Schickling, D. Schüttemeyer, F. Zemek, and U. Rascher, "Red and far-red sun-induced chlorophyll fluorescence as a measure of plant photosynthesis," *Geophysical Research Letters*, 2015.

[26] I. The MathWorks. (2016) Solve nonlinear least-squares (nonlinear data-fitting) problems. [Online]. Available: http://www.mathworks.com/help/optim/ug/lsqnonlin.html

[27] ——. (2016) Compare model output and measured output - matlab compare. [Online]. Available: http://www.mathworks.com/help/ident/ref/compare.html

[28] P. M. Van den Hof, "Model sets and parametrizations for identification of multivariable equation error models," *Automatica*, vol. 30, no. 3, pp. 433–446, 1994.

A

Derivation of Fraunhofer Line Discrimination equations

The FLD method rests upon the assumption that the ratio between radiance inside and outside the absorption band is equal for incident and reflected (superscript R) sunlight:

$$\frac{E_i}{E_o} = \frac{E_i^R}{E_o^R} \tag{A.1}$$

The quantities E_j^R, $j \in \{i,o\}$, added with chlorophyll fluorescence F, are measured by a spectrometer (radiances L_j):

$$\frac{E_i}{E_o} = \frac{L_i - F}{L_o - F} \tag{A.2}$$

Extracting F from the equation yields:

$$F = \frac{E_o L_i - E_i L_o}{E_o - E_i} \tag{A.3}$$

This equation is the base of a plethora of methods which improve upon it. One such method is 3FLD, which does not assume constant fluorescence over the absorption band, and furthermore accounts for the fact that the reflectance differs slightly over the interval concerned. Moreover, 3FLD compensates for the effects of path reflected radiance L_j^p and atmospheric transmittance τ_j to enable measurements from very high altitudes. This is described by the two relations below, where A and B are assumed constant.

$$F_i = BF_o, \quad R_i = AR_o \tag{A.4}$$

The measured radiance, inside and outside the absorption band, is modeled as below based on a radiative transfer model [11]. Surface reflectance is assumed to be Lambertian. τ_j represents upward transmittance for the distance from surface to sensor, R_j the reflectance and S_j the atmospheric spherical albedo (the term S_jR_j is the portion of sunlight which is reflected by the surface and then backscattered into the sensor by the surrounding atmosphere).

$$L_j = L_j^p + \frac{1}{\pi}\frac{(E_j^R + F_j)\tau_j}{1 - S_jR_j}, \quad E_j^R = R_jE_j, \quad j \in \{i,o\} \tag{A.5}$$

E_j^R is not available as a pure measurement, and so the reflectance R_j cannot be calculated exactly. However, an approximation can instead be made using the apparent reflectance $\tilde{R}_j$, in order to find A:

$$R_j \approx \tilde{R}_j = \frac{L_j}{E_j} = \frac{E_j^R + F_j}{E_j} \tag{A.6}$$

As the quantity $\tilde{R}_j$ depends on F_j to a greater degree in the absorption band, its value is not calculated from L_i and E_i directly but instead deduced through linear interpolation between the two shoulder bands:

$$R(\lambda) \approx a_1\lambda + a_2 \tag{A.7}$$

The parameters a_1 and a_2 are calculated by using one point on each side of the absorption band, $\lambda_1 = 753$ nm and $\lambda_2 = 771$ nm, based on the apparent reflectance $\tilde{R}$.

$$a_1 = \frac{\tilde{R}(\lambda_2) - \tilde{R}(\lambda_1)}{\lambda_2 - \lambda_1}, \quad a_2 = \tilde{R}(\lambda_1)\frac{\lambda_2}{\lambda_2 - \lambda_1} - \tilde{R}(\lambda_2)\frac{\lambda_1}{\lambda_2 - \lambda_1} \tag{A.8}$$

From this we can calculate A, inserting $\lambda_3 = 760$ nm into Equation (A.7), as

$$A = \frac{R(\lambda_3)}{R(\lambda_1)} \approx \frac{\tilde{R}(\lambda_1)C_1 + \tilde{R}(\lambda_2)C_2}{\tilde{R}(\lambda_1)} \tag{A.9}$$

where

$$C_1 = \frac{\lambda_2 - \lambda_3}{\lambda_2 - \lambda_1}, \quad C_2 = \frac{\lambda_3 - \lambda_1}{\lambda_2 - \lambda_1} \tag{A.10}$$

Using atmospheric modelling software, S_j, τ_j and L_j^p can be calculated. Consequently, what remains are four unknowns R_i, R_o, F_i, and F_o. In the interest of brevity, we first introduce X_j:

$$X_j = \pi \frac{L_j - L_j^p}{\tau_j} \tag{A.11}$$

Inserting into Equation (A.5) yields the top two equations in the following system of equations for the four variables:

$$\begin{cases} X_i = \frac{R_i E_i + F_i}{1 - S_i R_i} & (1) \\ X_o = \frac{R_o E_o + F_o}{1 - S_o R_o} & (2) \\ F_i = B F_o & (3) \\ R_i = A R_o & (4) \end{cases} \tag{A.12}$$

We can separate R_o from (2) in Equation (A.12), using (3) to eliminate F_o:

$$R_o = \frac{X_o - F_i B^{-1}}{E_o + S_o X_o} \tag{A.13}$$

Inserting Equation (A.13) into (1) from Equation (A.12), while using (4) to eliminate ρ_i, yields

$$X_i = \frac{A \frac{X_o - F_i B^{-1}}{E_o + S_o X_o} E_i + F_i}{1 - A \frac{X_o - F_i B^{-1}}{E_o + S_o X_o} S_i} \tag{A.14}$$

Now, we can express the fluorescence inside the absorption band by rearranging the equation to only have F_i on the left side:

$$F_i = B \frac{X_i(E_o + S_o X_o) - A X_o(E_i + S_i X_i)}{B(E_o + S_o X_o) - A(E_i + S_i X_i)} \tag{A.15}$$

B

Estimation of reference model

Using the measurements obtained without the presence of sunlight, a reference system was estimated as described by Lindqvist [13]. Only the second to the sixth step of Figure B.1 are used, with the others being disturbed by unwanted external factors (e.g. wind causing motion of the sun cover or plant canopy).

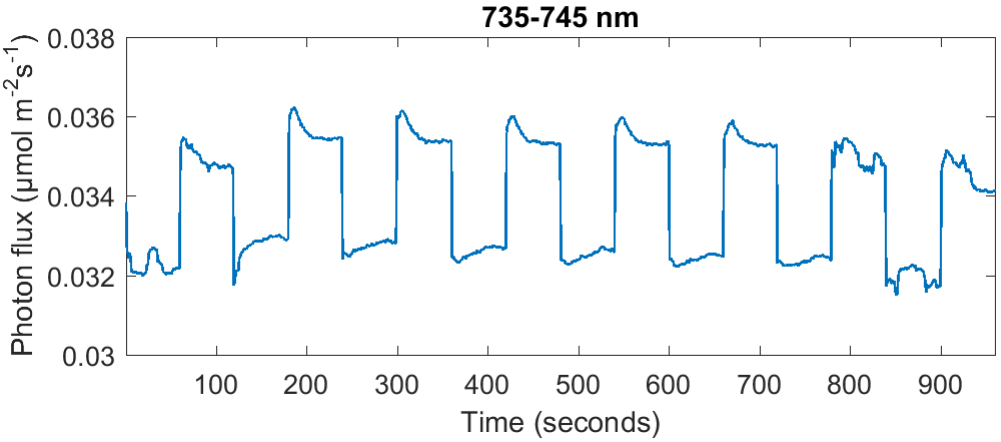

Figure B.1: Fluorescence in the interval between 735 nm and 745 nm, as measured by the downward facing spectrometer. The measurements are obtained without the presence of sunlight, in order to have a reference model with which to evaluate the methods in this work. Background lighting with photon flux similar to the ambient sunlight is generated by a second lamp. Only the second through sixth steps are used to generate the reference model, as the others are clearly disturbed by e.g. undesirable motion of the sun cover.

Figure B.2 shows the OE models fitted to the five selected step responses. A model structure with three poles and three zeros is used, motivated the relatively small influence of measurement noise enabling use of a higher model order (matching previous work by Lindqvist [13].

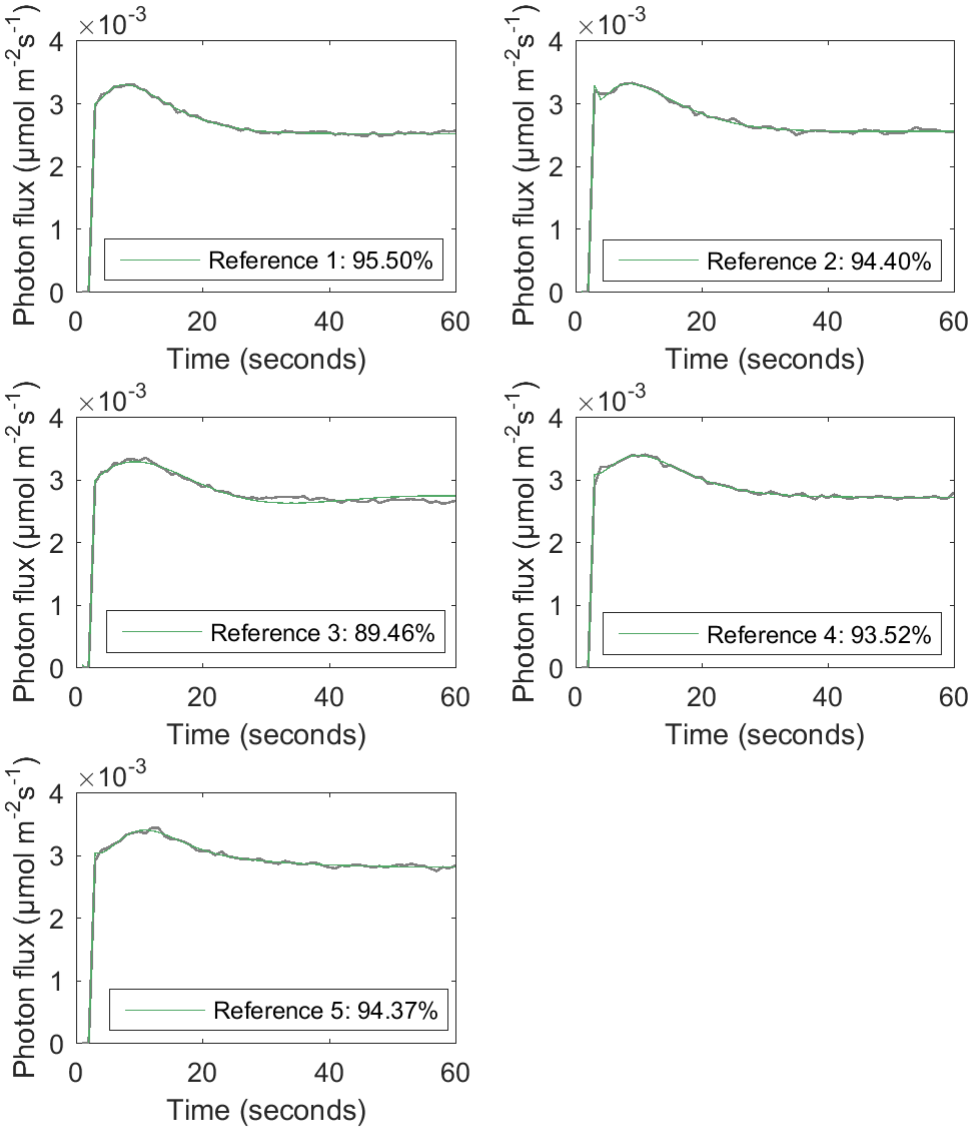

Figure B.2: OE430 models fitted to measured fluorescence responses.

The Bode diagrams of the five models can be seen in Figure B.3 as dotted black lines. The mean system, used in Chapter 4, is shown as a solid black line. It is calculated simply by taking the mean value of all five systems' magnitude and phase response, for the frequencies shown.

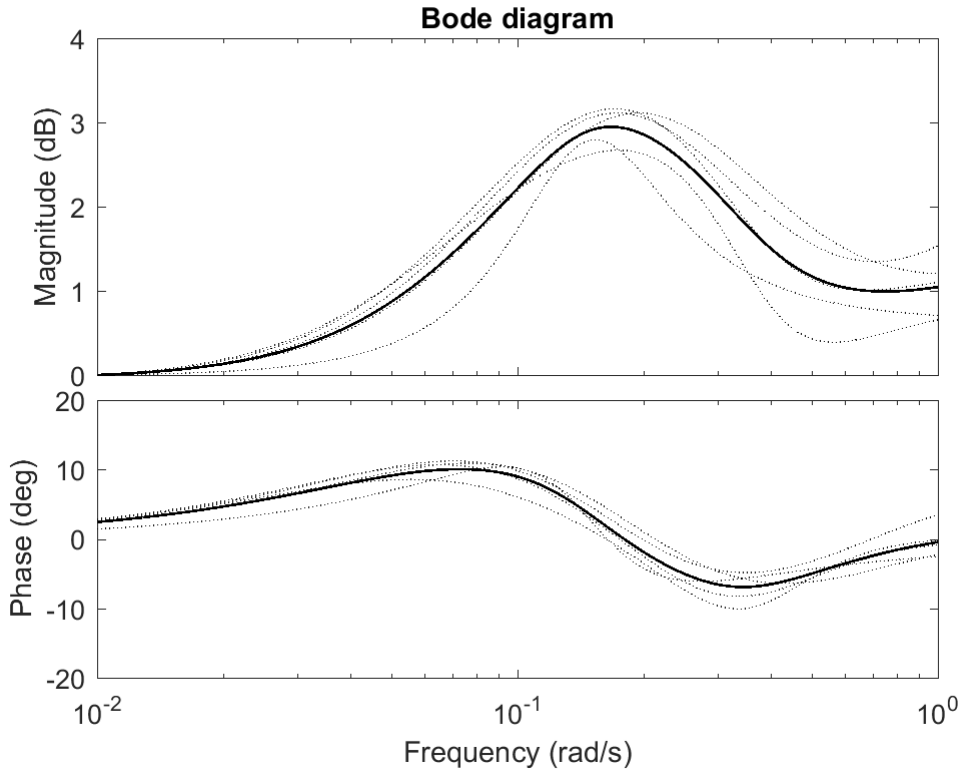

Figure B.3: Bode diagrams for the five estimated OE430 models (dotted), and the mean system (solid).

C

Least squares curve fitting

To further analyse the $\hat{\rho}$ resulting from the minimisation shown in Equation (3.24), the components of $y(n)$ and $u(n)$ can be written explicitly:

$$\min_{\hat{\rho}} \left(g(l(n) + d(n), t) + \rho d(t) - \hat{\rho} d(t)\right)^2 \tag{C.1}$$

This gives a $\hat{\rho}$ minimizing the expression as

$$\hat{\rho} = \rho + \frac{g(l(t) + d(t), t)}{d(t)} \tag{C.2}$$

It is clear that $\hat{\rho}$ is not a precise estimation of ρ, but depends also on the ChlF response. However, as the fraction in Equation (C.2) is much smaller than the reflectance (typically in the order of thousandths), the approximation can be used in situations where the sunlight is sufficiently large to warrant its use.

To perform the minimisation described by Equation (3.24), the problem is structured as an optimisation:

$$\begin{aligned} &\text{minimise} && \tfrac{1}{2}\|Y - Dx\|_2^2 \\ &\text{s.t.} && Ax \leq B \\ & && x \geq 0 \end{aligned} \tag{C.3}$$

with

$$x = [\hat{\rho}\ m], \quad Y = [y_1\ \cdots\ y_N]^T \quad B = [1\ Y^T]^T$$

$$D = \begin{bmatrix} d_1 & -1 \\ \vdots & \vdots \\ d_M & -1 \\ d_{M+1} & 1 \\ \vdots & \vdots \\ d_N & 1 \end{bmatrix}, \quad A = \begin{bmatrix} 1 & 0 \\ & D \end{bmatrix} \tag{C.4}$$

where the subscripts $1, ..., N$ denote sample number, N is the number of samples in a single step, m is the slack variable, and M is the last sample before the step (close, but not exactly equal to $\frac{N}{2}$).